17th AIAA/CEAS Aeroacoustics Conference (32nd AIAA Aeroacoustics Conference)
05 - 08 June 2011, Portland, Oregon

AIAA 2011-2788

Tailored Nozzles for Jet Plume Control and Noise Reduction

K. Viswanathan,[*] P. R. Spalart,[†] M. J. Czech[‡]
The Boeing Company, Seattle, Washington 98124

A. Garbaruk[§] and M. L. Shur[**]
New Technologies and Services and St. Petersburg State Polytechnic University
St. Petersburg 197198, Russia

A synergistic utilization of computational simulations with experimental measurements is employed to develop dual-stream nozzle geometries that provide jet noise reduction with the concurrent ability to control the orientation of the jet plumes, so as to minimize the thrust degradation associated with low-noise designs. The geometries consist of round primary and secondary nozzles, beveled primary nozzles, modified secondary nozzles, and combinations thereof. Specifically, the secondary nozzle is altered internally to provide the same deflection as a beveled primary in dual-stream exhaust geometry. The cross-sectional profiles are similar, but the bevel deflects the jet towards the short lip, whereas the modified secondary deflects the jet in the opposite direction. It is possible to eliminate/minimize the deflection of the total thrust vector through a judicious combination of the bevel and the modified secondary; numerical simulations facilitate this objective. The aeroacoustic characteristics of four beveled nozzles with bevel angles of 18º, 24º, 30º and 36º, and two modified secondary nozzles with weak and strong flow effects, have been established in a wind-tunnel test, with simultaneous measurement of thrust and noise. The magnitude of the noise reduction increases with increasing primary jet velocity and decreases with increasing flight Mach number. There is a gradual erosion of noise benefit as the azimuthal angle is increased from 0º (below the long lip of bevel). There is a benefit in EPNL for all the nozzle geometries evaluated in this investigation. The combinations of modified secondary nozzles with bevel24 and bevel30 provide the largest reduction in EPNL over a wide range of freestream Mach number, with a small thrust penalty. The noise benefit varies from ~2.5 EPNdB at Mt=0.0, to ~2.0 EPNdB at Mt=0.20, and ~1.2 EPNdB at Mt=0.28. The design approach developed and evaluated here seems promising vis-à-vis practical applications, requiring only relatively limited modifications to an existing design.

I. Introduction

A joint computational and experimental program is carried out to assess the flow and noise characteristics of dual-stream nozzles. The geometries consist of round primary and secondary nozzles, beveled primary nozzles, modified secondary nozzles, and combinations thereof. The nozzles are designed in such a way as to allow maximum flexibility and interchangeability in the choice of primary and secondary nozzle combinations, so as to independently assess the effects of geometric variations on jet plume evolution and radiated noise. Ever since the introduction of the high bypass ratio turbofan engine with dual-stream nozzles, there have been attempts to reduce the radiated noise through geometric variations to the nozzle exit shapes. The interest here is in non-axisymmetric modifications on a larger scale. In addition to the establishment of the noise characteristics of dual-stream baseline circular nozzles since the 1970s, see Ref. [1-6] for a very brief list, there have been investigations of modified nozzles. One of the earlier studies is due to von Glahn and Goodykoontz [7], in which the primary and secondary nozzles were non-concentric, with a thicker secondary jet in the flyover plane (towards the ground). Their results from a coplanar geometry indicated that there was (1) minor spectral changes at the lower radiation angles (measured from the inlet), and (2) a large reduction at the high frequency portion of the spectra for radiation angles ≥ ~130º. Bhat and Wright [8] illustrated various geometric arrangements in their 1981 patent and showed that the noise levels were lower in the azimuthal direction that corresponded to the thicker secondary shear layer. .

[*] Boeing Technical Fellow, Tel: (425) 237-2773, e-mail: k.viswanathan@boeing.com. Associate Fellow AIAA
[†] Senior Technical Fellow, philippe.r.spalart@boeing.com, Member AIAA
[‡] Aeroacoustics Engineer, michael.j.czech@boeing.com, Member AIAA
[§] Associate Professor, agarbaruk@cfd.spbstu.ru
[**] Leading Research Scientist, mshur@cfd.spbstu.ru, Senior Member AIAA

The concept of providing a shielding low-speed layer for directional noise reduction has been re-visited periodically ever since. Majjigi et al. [9] evaluated the shielding idea in a free jet facility, with forward flight. They discovered that the large reduction observed for the static case is almost completely absent in the peak noise radiation sector, when a flight stream is introduced. Seiner and Krejsa [10] assessed the noise reduction potential of several designs for noise reduction. A few non-concentric nozzles were also evaluated in the 1990s as part of NASA's High Speed Civil Transport and Advanced Subsonic Technologies programs. More recently, Papamoschou [11, 12] examined the acoustic and aerodynamic characteristics of flows from separate flow dual-stream nozzles, in which the shear layers were thickened in the downward and sideline directions through the use of wedges, pairs of vanes, or flaps in the secondary flow. All these mechanisms for flow modifications were based on the principle of setting up a thicker shielding layer; another interpretation is that the merging of the inner and outer shear layers and the associated surge in turbulence are delayed and made more benign. Good noise reduction was observed with all these geometric additions; noise benefits in the Effective Perceived Noise Level (EPNL, EPNdB) of 2.1 EPNdB in the downward direction and 1.0 EPNdB in the sideline directions were reported. Zaman et al. [13, 14] tested the same concepts at NASA Glenn; the geometries were identical to those in Ref. [11, 12], but eight times larger. They found some noise benefit for jets with low to moderate bypass ratios (BPR). However, the magnitude of noise benefit was found to be substantially lower for the bigger scale nozzle at NASA Glenn. All of these studies were restricted to static jets.

Bridges and Henderson [15] and Brown et al. [16] assessed the above concepts of vanes and wedges, along with the shaping of the fan flow (called S-duct in their terminology) at NASA Glenn and provided a comprehensive evaluation of offset stream technologies. Our design of the secondary nozzle to adjust the offset streams has similarities with the S-duct. The notable aspect of this program is a realistic evaluation with a forward flight stream. Furthermore, the offset stream concepts were examined at three bypass ratios of 5.0, 8.0 and 13.0, with measurements of flow and noise. Acoustic data were acquired both at static condition and with a tunnel Mach number (Mt) of 0.2. Cross-sectional profiles of the flow confirmed the thickening shielding layer in the downward direction as intended. A noise benefit at static conditions was observed at the lower bypass ratios. However, there was substantial increase of the spectral level at the higher frequencies, especially over a wide range of lower polar angles with forward flight. In the important metric of Effective Perceived Noise Level, the noise benefit completely disappeared with the addition of a flight stream for all the concepts and at all the bypass ratios. Figure 1, reproduced here from the NASA Glenn test, summarizes the main findings. This test program produced definitive trends and represents the status of the offset stream technologies. In addition, the importance of evaluating any noise reduction concept under realistic conditions is highlighted once again. This state of affairs brings us to the current study, which is described in the following section

II. Scope of Current Study

The above ideas for shielding rely on modifying the fan or secondary stream to produce a thicker fan layer in the desired azimuthal directions. Viswanathan [17-19] recently reported on the noise benefits that can be obtained with beveling the primary nozzle. Good noise reductions were observed for both single-stream and dual-stream nozzles; for dual-stream nozzles, the secondary nozzle was unaltered. Substantial noise reduction in the peak noise radiation sector was demonstrated for both single and dual jets, in the angular range $\geq$~120º. Further, there was no noise increase at the higher frequencies, in contrast with chevron nozzles. Noise benefit in EPNL, though lower with forward flight, was realized even with a flight Mach number of 0.32. See Figure 17 in Ref. [18]. There is a key difference between the beveled nozzle and the shielding concepts, as discussed by Viswanathan [18] in Section IV.B (page 624). It is important to realize that for a single jet, there is no "thickening" layer (or any layer for that matter) surrounding the jet. Yet, dramatic reductions in noise have been measured below the longer lip of the beveled nozzle. Therefore, the physics of noise reduction is very different for the beveled nozzle and is in no way connected to the shielding concepts that have been attempted in the last thirty years.

A detailed RANS and LES computational study of single-stream and dual-stream beveled nozzles, along with those of round nozzles, was carried out to gain better insights into the flow features responsible for noise reduction; see Viswanathan et al. [20] for complete details. Two sample flowfield results from Ref. [20] illustrate the differences in the jet evolutions. Figure 2 shows the instantaneous vorticity fields in the symmetry plane of the LES for the three nozzle geometries; the secondary nozzle is round for all three cases and the primary nozzle consists of a round nozzle, and two bevels with bevel angles (measured from the vertical nozzle exit plane for the round nozzle) of 24º and 45º, respectively. Aside from the plume vectoring, there is significant alteration of the turbulence structure of the jets. The fan streams of the beveled nozzles are highly asymmetric with the "top" being narrower and the

"bottom" substantially thicker than those for the round jets, after the top one begins merging with the core shear layer; this effect is much stronger for the bevel45 system. The fan flow needs to accommodate the upwards deflection of the core stream, which stretches it on the upper side, resulting in this thinning of the shear layer; conversely, there is lateral streamline convergence and thickening on the lower side. The modifications to the potential-core lengths are also highlighted by the vorticity fields: (1) as for the single jets, the length of the primary potential core is reduced as the bevel angle is increased, (2) the length of the secondary shear layer at the top is progressively shortened with increasing bevel angle, and (3) the behavior of the bottom shear layer is different for the two beveled nozzles; it is somewhat longer than the round for bevel24, and shorter than the round for bevel45 due to the rapid widening of the outer shear layer. In the above description, the secondary potential core is defined as the flow area between the two streams, free of vortical structures.

Several interesting features are observed, when the cross-sectional contours of vorticity from the RANS computations at several axial stations are examined for the static case in Figure 3. For the conventional nozzle, there are of course concentric rings of vorticity, mainly concentrated in the shear layers in the early mixing layers. As the flow evolves, these get gradually mixed out but retain their axisymmetric shape at all downstream locations. For the beveled nozzles, the region of high vorticity migrates towards the shorter side of the beveled nozzle and the plume gets elongated in the vertical plane. The fan flow (mixed with the ambient air) gets pulled towards the center of the core jet and the primary shear layer takes on a 'C shape'. The secondary shear layer is highly asymmetric, much thicker at the bottom, as also seen in the plots of instantaneous vorticity from the LES in Figure 2. Additional information may be found in Ref. [20].

The interesting flow features displayed in Figures 2 and 3 contrast the different evolutions of the jet plumes. Now, one could produce nearly the same flow cross-sectional patterns without beveling the primary nozzle, but through suitable shaping of the secondary nozzle. It is important to keep in mind that the precise mechanisms responsible for the generation and radiation of sound from high Reynolds number turbulent flows are not completely known, and the causal connection between flow/turbulence and noise generation has yet to be established quantitatively. This point is discussed in greater length in Ref. [20]. However, the approach taken here is to design a dual-stream nozzle system with a round primary nozzle that mimics the flow features observed in Figures 2 and 3. Two such secondary nozzles, here after referred to as modified fan nozzles MF1 and MF2 have been designed using the computational procedure. MF1 produces a weaker effect and MF2 produces a stronger effect. In the initial study of beveled nozzles by Viswanathan [17-19], no attempt was made to control the plume deflection; rather, the deflection angles for the various geometries and cycle conditions were established from the force measurements obtained with a six-component force balance. As seen in Figures 2 and 3, the plume deflects towards the short lip of the beveled nozzle for convergent beveled nozzles at all nozzle pressure ratios (NPR). One could tailor the secondary nozzles MF1 and MF2 in such a way as to counteract the plume deflection caused by a beveled primary nozzle and precisely align the total thrust axis. Regardless of the noise reduction potential of a modified secondary nozzle, now there is a way to control the jet plume with any given beveled primary nozzle. This would make the application to an existing design less disruptive; the deflection of the fan stream could also weaken jet-flap interaction.

A detailed aeroacoustic wind-tunnel test has been carried out to address the following questions: (1) would a modified secondary nozzle yield noise reduction by itself? (2) if so, would the noise benefit together with a beveled primary nozzle be additive? (3) can the thrust alignment be controlled with this design approach? (4) does the noise reduction correlate well with flow features in steady CFD solutions (as opposed to large-eddy simulation), such as the relative positions of shear layers? This fourth point would be most helpful in industrial practice, for installed engines. From a practical standpoint, it was decided to create a wider database with four different primary beveled nozzles with bevel angles of 18º, 24º, 30º and 36º and two modified secondary nozzles. MF1 produces a "weaker" deflection and MF2 a "stronger" deflection in a direction opposite to those of the beveled nozzles. An equivalent round nozzle system was employed to generate baseline data for comparison. Aeroacoustic data have been generated with all possible combinations of baseline and modified nozzles. Results from the experimental study, together with computed flow fields, are presented in this paper.

III. Overview of Computational Procedure

The numerical system developed by Shur et al. [21-23] is utilized for the investigation of the aeroacoustics of the nozzles considered. Therefore, only a brief overview of the prediction procedure is needed here. A high-order computer code, described by Strelets [24], is run on structured multi-block curvilinear grids. The versatility and the

robustness of the code were demonstrated for a variety of aerodynamic flows and excellent comparisons with benchmark experimental data were shown in Ref. [24]. For jet noise predictions, the turbulence is treated by LES and the farfield noise is computed with the Ffowcs-Williams/Hawkings (FWH) [25] formulation. The Navier-Stokes equations are solved with a slightly upwind-biased high-order differencing for spatial discretization and implicit time integration. The time integration is carried out with a second order three-layer backward scheme and dual time stepping. In the turbulent flow region and in the near field the spatial discretization utilizes a combination of fourth-order centered and fifth-ordered upwind-biased scheme, based on flux-difference splitting for the inviscid terms. Outside this region, purely upwind differencing is employed to damp out the outgoing waves. A buffer layer, in addition to non-reflecting boundary conditions, is included to ensure that reflections from the boundaries do not contaminate the solution in the domain of interest. For simulating the turbulence, the Sub-Grid-Scale (SGS) model is de-activated, and the approach is viewed as "Implicit LES". The slight dissipation introduced by the upwind scheme (with a typical weight of 0.25) serves the purpose of removing the energy that would be transferred to the unresolved scales as part of the energy cascade. Several other approaches were evaluated as well; this choice turned out to be the best option for simulating realistic transition to turbulence, as explained in Ref. [21-23].

The computations are performed with the use of the ν_t-92 model, which is a one-equation linear isotropic eddy-viscosity transport model developed since the 1970s by Secundov [26, 27], and is more attractive than other common models for round jets because of a correction term activated by the curvature of the eddy-viscosity contours (however, this becomes active in the fully-developed jet region, not in the thin mixing layers which separate the potential cores). It also contains a compressibility correction, which is felt in sonic mixing layers. We note that the complexity in the present flows is primarily inviscid in nature: transverse pressure gradients and compressibility on the potential core. The boundary layers remain thin and attached thanks to the contraction, so that the impact of turbulence-modeling imperfections is slight.

IV. Experimental Program

The aeroacoustic test has been carried out at Boeing's Low Speed Aeroacoustic Facility. Detailed descriptions of the test facility, the jet simulator, the data acquisition and reduction process, etc., may be found in Ref. [28, 29]. For the sake of completeness, a brief overview is provided here. Bruel & Kjaer quarter-inch Type 4939 microphones are used for free-field measurements. The microphones are set at normal incidence and without the protective grid, which yields a flat frequency response up to 100 kHz. Typically, several microphone arrays are used; these arrays are at a constant sideline distance of 15 ft (4.572 m) from the jet axis and on a polar arc of 25 ft (7.62 m). All angles are measured from the jet inlet axis, and cover a polar range of 50º to 150º. Very fine narrow band data with a bin spacing of 23.4 Hz up to a maximum frequency of 88,320 Hz are acquired and synthesized to produce one-third octave spectra, with a center band frequency range of 200 Hz to 80,000 Hz. The jet simulator is embedded in a free-jet wind tunnel, which can reach a maximum Mach number of 0.32. The dimension of the wind-tunnel is 9 ft by 7 ft. The jet simulator is incorporated with a six-component force balance and simultaneous measurements of thrust and noise are acquired.

The diameter of the baseline primary nozzle is 2.08" and the area ratio between the secondary and primary nozzles (As/Ap) is 3.92. The subscripts p and s denote primary and secondary, respectively. Recall that convergent beveled nozzles were tested in Viswanathan [17] and are also used here. From the experimentally measured actual mass flow rate for given plenum conditions with a critical flow venturi, it was established in Ref. [17] that the effective flow area for the beveled nozzles is lower than the geometric area (in the slant plane). This reduction in flow area is attributable to non-uniform pressure distribution at the exit plane and has been confirmed with numerical simulations in Ref. [20]. The center plug in the dual-stream nozzle geometry tested could be moved in the axial direction, thereby providing ability to control and set the annulus flow area. In the current test program, CFD (computational fluid dynamics) simulations for the four beveled nozzles were first carried out and the computed mass flow rates for the four beveled nozzles were compared with the corresponding mass flow for a round nozzle, for fixed plenum conditions. Based on the reduction, the exit area for each beveled nozzle was increased by suitably setting the annulus flow area such that the mass flow rate matched that of the round nozzle. It was also verified through CFD simulations that the mass flow rates for the modified fan nozzles matched the mass flow rate for the baseline round secondary nozzle; the discrepancies in mass flow rates were $\leq 0.3\%$ for all geometries. In strict terms, the secondary flow path is altered in the desired fashion without modifying the exit area, using slight S-shaping upstream. Thus, the nozzle exit areas were chosen to produce the same mass flow rates for all the nozzles.

V. Computed Flowfields

Sample flow computations are presented in order to highlight the changes to the flowfield due to modifications of the nozzle geometries and emphasize the approach for controlling the jet plume and presumably reducing its noise. An extensive set of nozzle geometries, both primary and secondary, were considered and analyzed with RANS computations prior to the decision to fabricate the four beveled primary nozzles and two modified secondary nozzles. First, we demonstrate that it is possible to produce the same flow features observed for the primary beveled nozzles (with round secondary) through suitable tailoring of the secondary nozzle alone (with round primary). Figure 4 shows side-by-side comparisons of contours of streamwise velocity in the cross-sectional planes; six different axial stations are considered. The jet operating conditions are as follows in all the computational results shown below: NPRp=NPRs=1.8, Tp/Ta=2.37, Ts/Ta=1.0 and Mt=0.20. The velocity contours for the baseline (round + round) are on the left hand side and the modified nozzles on the right. In Figure 4, contours are presented for the baseline and bevel24+round. The axial distance is normalized by the diameter of the secondary jet (D2). The evolution and spreading of the jet with downstream distance, with progressively larger cross-sectional areas are evident. Whereas the jet shape is concentric for the baseline, the increasing distortion and stretching of the jet in the vertical plane produce an oval shape for the bevel24 primary nozzle. The deflection of the jet towards the short lip of the beveled nozzles (towards the top in the figure) is also obvious; the trends are similar to those seen in Figure 3. Figure 5 shows a comparable flowfield obtained through the modification of the secondary nozzle alone. Note that the flow is deflected downward, but the gross features are similar to those seen in Figure 4. For instance, the plume shape is oval, with stretching in the vertical plane and progressive distortion with increasing downstream distance. Let us pay closer attention to the contours in Figures 4 and 5 at x/D2=6: the contour shapes of different velocities and corresponding areas are similar.

Next we consider a larger bevel angle of 45° and a correspondingly larger deflection of the plume in Figure 6. As expected, the effects of this larger bevel angle are more pronounced than those of bevel24. An equivalent flowfield obtained through the modification of the secondary nozzle is shown in Figure 7; the degree of nozzle modification is larger to closely duplicate the larger effect due to bevel45. Again, the flow features are comparable. It is clear that the design procedure adopted for modifying the secondary nozzle alone produces similar flow features obtained through the beveling of the primary nozzle and a round secondary nozzle. Notice though that the plume deflection is in the opposite direction.

Sample computed flows with combinations of different beveled primary nozzles and modified secondary nozzles are now presented to illustrate the ability to control the plume vectoring. An examination of the variation of axial velocity in the symmetry plane of the jet, with downstream distance, highlights the various effects. Such a variation is depicted in Figure 8 for the baseline, bevel45, strongly modified secondary, and a combination of bevel24 + modified secondary nozzles. These axial contours indicate that the bevel deflects the plume upwards, the modified secondary deflects the plume downwards, and the combination more or less aligns the jet plume with the x-axis. The reduction in potential core lengths for all the modified nozzles, when compared with the baseline nozzle, is also evident. A comparison of the baseline and (bevel24 + modified secondary) highlights the stark differences in the flowfields between the two geometries, though the plumes are aligned with the x-axis.

The degree of modification to the secondary nozzle is controlled by a geometric parameter; the higher the value of this parameter, the larger the plume deflection. The criterion for plume alignment with the x-axis is the following: find a suitable value for this parameter that would reduce the vertical force to zero or within a small tolerance. This exercise was carried out for three bevel angles of 15°, 20° and 24°. The computed normal forces were $\leq 0.08\%$ for all cases. The resulting computed flowfields in the cross-section planes are shown in Figures 9 – 11, respectively, for the three bevel angles. The increasing distortion of the plume with increasing degree of modifications, due to larger bevel angle and compensatory alteration of the secondary, are evident in these figures. Further, the centroids of the jet plumes are located close to the jet centerline (x-axis). Thus, the ability to control the jet plume for any given beveled primary nozzle with a suitable offsetting effect induced by the modified secondary nozzle has been demonstrated. The noise characteristics of these nozzle geometries will now be evaluated.

VI. Experimental Results

The salient results from the aeroacoustic test program are presented in this section. First, the aerodynamic performance of the various nozzle combinations are presented and discussed. The acoustic results are then highlighted using several noise metrics.

A. Aerodynamic Performance

Particular attention is paid to the thrust measurements, given the importance of quantifying and controlling the plume deflection angle with the various nozzle geometries. The force balance was calibrated by applying a known force and measuring the response of the balance. The applied force was incremented by 100 lbf, starting from 0 lbf to 1400 lbf. Then the applied load was decreased 100 lbf step-wise, so as to document hysteresis effects, if any. This exercise was carried out twice, the first time before the start of the test and the second time after the completion of the test. Figure 12 shows the calibration curve; there are two sets of circles (pre-test calibration) and two sets of triangles (post-test calibration). The straight line is the ideal response, with a 45º slope. As seen, there is excellent linear response and the average error for the calibration is ± 0.13%. In general, the maximum error in the thrust measurements can be taken to be less than ± 0.20%, though it can be actually lower. Additional information may be found in Section III.B of Ref. [28]. The measured thrust is used to calculate the thrust coefficient using the gas dynamic equations and standard procedure. This procedure involves the calculation of the ideal jet velocities in the two streams together with the measured mass flow rates for the determination of the ideal thrust. The thrust coefficient is the ratio of the measured thrust divided by the ideal thrust.

First, it is verified that the measured mass flow rates for the baseline and beveled nozzles are very close. This step is essential for noise differences to be meaningful. Figure 13 shows the variation of the corrected mass flow rate with nozzle pressure ratio. The corrected mass flow rate at standard ambient conditions is calculated from the measured mass flow rate using the usual definition. The trends for the beveled nozzles are very close to that of the baseline round nozzle. This level of agreement is deemed to be acceptable for this proof-of-concept test and therefore any fine tuning of the plug position is not carried out in the interest of test time. The plume deflection angle is calculated from the measured axial and normal forces. The sign convention for the deflection angle is as follows: when the deflection is towards the short lip of the beveled nozzle, the angle is taken to be positive; when the deflection is towards the long lip, it is negative. Figure 14 shows the measured deflection angles for all the nozzle geometries tested at maximum takeoff power: NPRp=1.71, Tp/Ta=3.16, NPRs=1.76, Ts/Ta=1.24. The modified secondary nozzles, in conjunction with the round primary nozzle, deflect the plume downwards; the deflection angle is larger for the stronger modification, as expected. The deflections due to the beveled nozzles, in conjunction with the round secondary nozzles, increase progressively with increasing bevel angle: from ~1° for bevel18 to ~2.2° for bevel36. Again, the expected trends are manifested in the measurements. The vertical chain lines demarcate the different beveled nozzles in Figure 14. The combinations of the modified nozzles with the bevels produce the desired reduction in the plume deflection angle: the stronger the modification to the secondary, the larger the reduction in the deflection angle. Similar trends for plume deflection are observed in Figure 15 at cutback power: NPRp=1.38, Tp/Ta=2.74, NPRs=1.56, Ts/Ta=1.16. The measured trends are in accord with the plume characteristics observed in the CFD simulations and confirm the efficacy of the design philosophy. It is not at all surprising that the bevel36 produces the maximum plume deflection. However, that is not the optimum bevel angle for noise, as will be seen. In general, the values of the deflection angle are within ± ~1.5°. The cosine of 1.5° is 0.99966, so that the thrust loss is negligible. It is important to keep in mind that there is no single-point design for a particular bevel angle; rather, combinations of bevel angles and modifications to the secondary are evaluated so as create a database.

The propulsive performance of the various nozzle geometries is next assessed. It is easier to observe the effect of nozzle modifications through the examination of the difference in thrust coefficient relative to that of the baseline nozzle system. Figures 16 and 17 show such variations at maximum takeoff power and cutback power, respectively. The nozzle with the largest bevel angle produces the largest thrust loss relative to the baseline. In general, the combinations of bevel24 and bevel30 with the modified nozzles lead to relatively low thrust degradation, nearly within the experimental measurement error. These results suggest that it should be possible in theory to design a dual-stream nozzle system with acceptable performance penalty for a desired beveled primary nozzle.

B. Acoustics

The acoustic performance of the various nozzle geometries is assessed now. The as-measured spectra are converted to lossless conditions for comparisons at model scale. The method proposed by Shields and Bass [30] is used to calculate the atmospheric absorption coefficients, which are frequency dependent. For the test conditions with forward flight, the method due to Amiet [31, 32] is employed to correct for the convection of the acoustic rays by the tunnel flow and the refraction due to the tunnel shear layer. The changes in the spectral amplitude and the radiation angle due to the co-flow have been calculated using this procedure. An interpolation of the resulting spectra at the true radiation angles to the radiation angles for the static case (fixed microphone angles) allows the direct comparison of the spectra obtained at various tunnel Mach numbers. For engine scale comparisons, the model scale spectra are extrapolated to full-scale conditions with a level flight for the aircraft at a fixed altitude of 1000 ft. Lossless spectral comparisons as functions of raw frequency in Hertz are presented in the following figures.

1. Jets in Static Environment

The efficacy of the modifications to the secondary nozzle vis-à-vis noise reduction is first evaluated. For the sake of clarity, the definitions of various angles viz. polar (χ), azimuthal (ϕ) and bevel angle (θ) are identified with a sketch in Figure 18. Spectral comparisons at four polar angles of 90°, 130°, 140° and 150° are shown in the following figures; an examination of a large set of data indicates that the changes to the spectra at the lower polar angles are relatively minor and the spectral changes at 90° can be taken to be representative of the trends at all the lower polar angles in the forward quadrant. Figure 19 presents a comparison of the spectra obtained with the baseline (round + round), round + MF1, round + MF2, and bevel24 + round; the jet conditions are NPRp=1.55, Tp/Ta=3.0, NPRs=1.71, Ts/Ta=1.21. The azimuthal angle (ϕ) is 0°, as when the observer is directly below the aircraft. There are only minor changes at 90°. Both the modified secondary nozzles yield noise reductions in the peak radiation sector at large aft angles. Thus it is verified that the modified secondary nozzles do provide a noise benefit in the peak radiation sector. But the magnitude of reduction is much smaller than is obtained with bevel24. When the engine power is increased to NPRp=1.71, Tp/Ta=3.16, NPRs=1.76, Ts/Ta=1.24 in Figure 20, the noise reductions due to MF1 and MF2 are enhanced slightly; however, the larger magnitude of reduction at the higher power for the bevel24 is not observed for the modifications to the secondary nozzle.

The reason for the lower noise benefit obtained with the modifications to the secondary becomes apparent when the azimuthal variation is examined. Figures 21 and 22 show spectral variations at the same four polar angles but at ϕ = 0°, 30° and 60°, for the round + MF2 and Bevel24 + round, respectively. The jet operating conditions are NPRp=1.71, Tp/Ta=3.16, NPRs=1.76, Ts/Ta=1.24. There are some blips in the spectra at 150° at ~250 Hz, for the microphones at azimuthal angles of 30° and 60°; these blips are caused by reflections from the exhaust collector, as explained by Viswanathan [29]. Note that for the microphone arrays at constant fixed sideline distance, the axial microphone locations at 150° are closer to the exhaust collector. These tones should be ignored, as they are not part of the changes to the noise due to nozzle modifications. First of all, the noise level increases in the peak radiation sector with increasing azimuthal angle for both geometries. It is also clear that the degree of azimuthal variation introduced by MF2 is much less pronounced (~2 to ~3 dB) when compared with that due to bevel 24 (~5 to ~6 dB). One could infer then that the lower noise benefit observed in Figures 19 and 20 is due to the weaker effect of MF1 and MF2 in introducing azimuthal variations in the spectra.

The noise benefit obtained with the different bevel nozzles (bevel angles of 24°, 30° and 36°) are quantified in Figures 23 and 24, for the two power settings of NPRp=1.55, Tp/Ta=3.0, NPRs=1.71, Ts/Ta=1.21 and NPRp=1.71, Tp/Ta=3.16, NPRs=1.76, Ts/Ta=1.24, respectively. In general, the noise benefit increases with increasing bevel angle; furthermore, the magnitude of noise benefit for a given bevel angle is larger for the higher power setting, with increased primary jet velocity. The observed trends at static conditions in the current test are consistent with the trends reported by Viswanathan [18].

2. Jets in Forward Flight

The effects of forward flight on noise of various geometries are assessed next. As for the static case, the noise potential of the modified secondary nozzles is first examined. Figure 25 presents a comparison of the spectra obtained with the baseline (round + round), round + MF1, round + MF2, and bevel24 + round; the jet conditions are NPRp=1.62, Tp/Ta=3.07, NPRs=1.74, Ts/Ta=1.22. The azimuthal angle (ϕ) is 0° and the freestream Mach number Mt=0.20. The spectral changes are again minor at 90°. In the peak directions, all the modified nozzles yield noise reductions. It is also worth pointing out that there is no increase at the higher frequencies, both for the static and wind-on cases. The power setting is increased to NPRp=1.71, Tp/Ta=3.16, NPRs=1.76, Ts/Ta=1.24 in Figure 26. Comparable spectral trends, but with larger noise reductions, are observed at this higher power. Once again, the bevel24 provides a larger noise benefit. Therefore, it is established that the design philosophy for the secondary nozzle modifications in which the flow cross-sections resemble those due to the primary bevel, provides noise benefit both for jets in static conditions and in the presence of a forward flight stream.

The noise characteristics of geometries with modifications to both nozzles are examined now. Spectral comparisons of the baseline (round + round) with bevel24 + round, and bevel24 + MF1 are shown in Figure 27. The jet operating conditions are NPRp=1.55, Tp/Ta=3.0, NPRs=1.71, Ts/Ta=1.21. The azimuthal angle (ϕ) is 0° and the freestream Mach number Mt=0.20. At 90°, there is negligible change. At lower polar angles (not shown), there is a slight increase in level. In the peak radiation sector, there is a ~3 dB to ~4 dB reduction in level over a large frequency range near the spectral peak, without increased levels at the higher frequencies. An immediate observation is the following: most of the noise benefit is provided by bevel24, with the addition of MF1 resulting in very minor changes.

Another comparison of the baseline with bevl30 + round, and bevel30 + MF1 is shown in Figure 28, at the higher power setting of NPRp=1.71, Tp/Ta=3.16, NPRs=1.76, Ts/Ta=1.24. The azimuthal angle (ϕ) is 0° and the freestream Mach number Mt=0.20. The observed spectral trends are similar to those seen in Figure 27. There is a larger noise benefit at the aft angles. Again, most of the noise benefit is provided by bevel30. The freestream Mach number is increased to 0.28 in Figure 29. The tail-up at the lower frequencies is due to contamination from the tunnel noise floor and is not related to the noise from the jet. At this higher Mt, there is noise increase at 90° and at the lower angles; as we move aft, spectral reductions are obtained. So far, attention has been restricted to ϕ = 0°. Now we examine the spectral characteristics at other azimuthal angles. Figures 30 and 31 depict comparisons for the same operating conditions, but at ϕ = 30° and 60°, respectively. At ϕ = 30° in Figure 30, there is a slight increase in level at 90°; there is still a larger noise reduction at the aft angles. At ϕ = 60° in Figure 31, the angular range over which noise reduction is observed is drastically reduced; even at 130°, there is an increase in levels at the higher frequencies, though there is some reduction at the lower frequencies. Similar trends are observed at other jet conditions (not shown). It is important to keep in mind that the nozzle designs investigated here are directional in character, in that noise reductions are obtained over a certain angular sector in the azimuthal plane. The benefit peaks at ϕ = 0° and gradually diminishes with increase in azimuthal angle. Such behavior has been reported by Viswanathan [18] for the primary bevel with a round secondary; given the minor spectral modifications introduced by the addition of a modified secondary nozzle, perhaps it should not be surprising that similar trends are observed for the combination of beveled primary with modified secondary nozzle.

Finally, the noise benefits are quantified at engine scale. As already noted, the measured spectra are extrapolated to engine scale, with a steady level flight for the airplane at an altitude of 1000 ft. The variation of the Perceived Noise Level (PNL, PNdB) with radiation angle provides a composite picture of the noise characteristics. Such a variation is presented in Figure 32 for the baseline, round + MF1, and bevel24 + MF2. The jet operating conditions are NPRp=1.62, Tp/Ta=3.07, NPRs=1.74, Ts/Ta=1.22. The azimuthal angle ϕ = 0° and the freestream Mach number Mt = 0.20. The modified nozzle MF1 by itself provides a slight reduction in PNL at the aft angles. The combination of bevel24 + MF2 results in a slight increase of ~1 dB at the lower polar angles; however, there is significant noise reduction of ~3 dB to ~4 dB at large aft angles. The benefits in the Effective Perceived Noise Level (EPNL, EPNdB) relative to the baseline are 0.54 dB and 1.2 dB, respectively, for these two modified geometries. Another sample variation of PNL is shown in Figure 33, for the baseline, bevel30 + round, and bevel30 + MF1. The jet operating conditions are NPRp=1.71, Tp/Ta=3.16, NPRs=1.76, Ts/Ta=1.24. The azimuthal angle ϕ = 0° and the freestream Mach number Mt = 0.20. At this higher power setting, the reduction in PNL is substantial in

the aft quadrant, for polar angles ≥ 120°. These trends are consistent with the spectral variations shown in Figure 29. Again, there is a slight increase in level at the lower polar angles. The noise benefits in EPNL for the two geometries are 2.0 EPNdB and 1.96 EPNdB, respectively.

The noise benefit, relative to the baseline, for all the geometries is presented at three freestream Mach numbers of 0.0, 0.20 and 0.28 in Figure 34. The jet operating conditions are NPRp=1.71, Tp/Ta=3.16, NPRs=1.76, Ts/Ta=1.24. The azimuthal angle $\phi = 0°$. For the static case, the noise benefit increases with increasing bevel angle; there is a reduction of 2.65 EPNdB for bevl36. This trend was observed in Viswanathan [18] as well. However, the introduction of a flight stream changes the achieved benefit for the different geometries. First of all, the benefit is reduced, which becomes more pronounced with increasing Mt. For example, for bevel30 + MF1, the noise reductions are 2.48, 1.96 and 1.22 EPNdB, respectively, at the three flight Mach numbers. A combined analysis of thrust performance and noise benefit, over a larger range of jet operating conditions, reveals that the optimum bevel angle is somewhere between 24° and 30°. The combinations of the modified secondary nozzles with the bevel24 and bevel30 primary nozzles provide the most noise benefit over a wide range of flight Mach numbers and lower thrust degradation. The large database generated in the current study may be used in conjunction with computational simulations to arrive at an optimum design for a desired bevel angle of the primary nozzle.

VII. Summary

A methodology for designing dual-stream nozzle geometries that provides jet noise reduction concurrently with the ability to control the orientation of the jet plume has been developed and evaluated in this joint computational and experimental investigation. The geometries consist of round primary and secondary nozzles, beveled primary nozzles, modified secondary nozzles, and combinations thereof. The nozzles are designed in such a way as to allow maximum flexibility and interchangeability in the choice of primary and secondary nozzle combinations, so as to independently assess the effects of geometric variations on jet plume evolution and radiated noise. The technology status of the effect of offsetting the secondary flow so as to produce a thickening shielding layer in the direction of desired noise reduction is reviewed: the main conclusions are, (1) some noise benefit is obtained in static situations, and (2) there is increase in the Effective Perceived Noise Level at all bypass ratios when a forward flight stream is introduced. It is emphasized once again that the mechanism associated with noise reduction due to a beveled primary nozzle is not related to the shielding concepts.

Computational simulations have been utilized to design modified secondary nozzles (in conjunction with a round primary nozzle) to produce the same cross-sectional patterns of the jet plume as produced by a beveled primary nozzle plus a round secondary nozzle. This objective is first demonstrated. The main difference between the two flowfields is the following: the bevel deflects the flow towards the short lip; the modified secondary deflects the flow in a diametrically opposite direction. Though the precise mechanism responsible for noise reduction by the beveled nozzle is not fully understood, it is at least possible to quantify and analyze the changes to the plume development through numerical simulations. (As an aside, it should be appreciated that the flow/noise causality is still an open question.) Such an endeavor served to underpin the design of the secondary nozzles. It has also been demonstrated through CFD that the combination of bevel + modified secondary can be precisely tailored for any desired bevel angle to eliminate the forces in a plane normal to the jet axis.

In the companion experimental study, four primary beveled nozzles with bevel angles of 18º, 24º, 30º and 36º and two modified secondary nozzles (MF1 and MF2) have been considered. MF1 produces a weaker deflection and MF2 a stronger deflection in a direction opposite to those of the beveled nozzles. The diameter of the baseline primary nozzle is 2.08” and the area ratio between the secondary and primary nozzles (As/Ap) is 3.92. The main objective of the experimental program is to create a wide database that can be used to answer the following questions: (1) would a modified secondary nozzle yield noise reduction by itself? (2) if so, would the noise benefit together with a beveled primary nozzle be additive? (3) verify experimentally that the thrust alignment can be controlled with this design approach. An equivalent round nozzle system has been employed to generate baseline data for comparison. Aeroacoustic data, with simultaneous measurement of thrust and noise, have been generated with all possible combinations of baseline and modified nozzles.

First, it is verified that the all the primary beveled nozzles have the same mass flow as the baseline round over a range of NPR; the flow path of the secondary nozzle is modified without altering the nozzle exit area. Therefore, all the nozzle combinations pass the same mass flow rates for fixed plenum conditions and produce approximately the

same absolute thrust. The experimental measurements confirm the expected trends of (1) deflection towards the short lip for the bevel, with progressively increasing deflection angle from ~1° for bevel18 to ~2.2° for bevel36; (2) deflection towards the long lip for the modified secondary, with MF2 producing a larger deflection; and (3) the combination of bevel + modified secondary counteracting the deflection due to the bevel alone and re-directing the jet plume towards the jet axis (and beyond), depending on the combination of the two nozzles. The thrust performance of a few of the nozzle combinations is within the error bar of the experimental measurements. In general, the largest bevel angle of 36º results in an unacceptably large thrust degradation and will not be suitable for practical application. It seems possible to design an acceptable nozzle system with a maximum bevel angle of ~30º and an appropriately designed modified secondary nozzle.

Under static conditions, both the modified secondary nozzles yield spectral reductions in the peak radiation sector in the aft quadrant. Thus it is verified that the flow patterns created by the modified nozzles with a round primary, which mimic the flow cross-sections of a beveled primary nozzle, can lead to noise reduction in the aft angles. However, the magnitude of noise reduction in the azimuthal direction of the long lip is much smaller than that achieved by the beveled primary. The reason for the lower magnitude of reduction due to the modified secondary can be gleaned through the examination of the azimuthal noise field: the degree of azimuthal variation at a fixed polar angle introduced by the modified secondary is much smaller than that induced by the bevel. Consequently, the noise reduction at a particular azimuthal angle is smaller in magnitude for the modified secondary. The magnitude of noise reduction increases with increasing bevel angle, for jets in a static environment.

Even with the introduction of forward flight stream, there is noise reduction for the modified secondary nozzles. Thus, one of the fundamental questions is answered: the modifications to the secondary nozzle as envisaged in this study are effective both at static and wind-on situations. Once again, the magnitude of noise reduction is much smaller than is obtained by the beveled primary. Most of the noise benefit for the combination of bevel + modified secondary is provided by the bevel alone; only minor spectral modifications are seen for the addition of the modified secondary nozzle to the beveled primary. The magnitude of the noise reduction increases with increasing primary jet velocity and decreases with increasing flight Mach number. There is a gradual erosion of noise benefit as the azimuthal angle is increased from 0°. These results are consistent with prior observations for dual-stream nozzles with beveled primary. The cumulative noise benefit for the various nozzle geometries is established through the calculation of the Effective Perceived Noise Level. An examination of the directivity of the Perceived Noise Level indicates that there could be a small increase in level, relative to the baseline, of ~ 1 PNdB at the lower polar angles in the forward quadrant; however, this small increase is more than overcome by significant noise reduction of ~3 to ~4 PNdB in the peak noise radiation sector, typically for polar angles $\geq$~120°. There is a net reduction in EPNL for all the nozzle geometries evaluated in this investigation. The combinations of modified secondary nozzles to bevel24 and bevl30 provide the largest reduction in EPNL over a wide range of freestream Mach number. The noise benefit at $\phi = 0°$ varies from ~2.5 EPNdB at Mt=0.0, to ~2.0 EPNdB at Mt=0.20, to ~1.2 EPNdB at Mt=0.28. These results, taken together with low thrust loss for these nozzle combinations, signify that the optimum bevel angle lies somewhere in this angular range from an aeroacoustic perspective. A point design for a modified secondary nozzle for a particular bevel angle in this desirable range is feasible with the design methodology developed and evaluated here. The synergistic melding of computational simulations with experimental measurements highlights the power of a joint approach and represents a significant step in nozzle design for noise reduction and low thrust penalty.

REFERENCES

1. Olsen, W.A., and Friedman, R., "Jet Noise from Coaxial Nozzles Over a Wide Range of Geometric and Flow Parameters," AIAA Paper 74-43, 1974.

2. Kozlowski, H., and Packman, A. B., "Aeroacoustic Tests of Duct-burning Turbofan Exhaust Nozzles," NASA CR-2628, 1976.

3. Tanna, H. K., Tester, B. J. and Lau, J. C., 1979 "The Noise and Flow Characteristics of Inverted-Profile Coannular Jets," NASA CR-158995, 1979.

4. Goodykoontz, J.H. and Stone, J.R., "Experimental Study of Coaxial Nozzle Exhaust Noise," AIAA Paper 79-0631, 1979.

5. Tanna, H. K., "Coannular Jets – Are They Really Quiet and Why?" Journal of Sound and Vibration, 72(1), 1980, pp. 97-118.

6. Lu, H. Y. "Effect of Excitation on Coaxial Jet Noise," AIAA Journal, Vol. 21, No. 2, 1983, pp. 214-220.

7. von Glahn, U. and Goodykoontz, J.H., "Noise Suppression Due to Annulus Shaping of a Conventional Coaxial Nozzle," NASA TM 81461, April 1980.

8. Bhat, V. W. and Wright, C. P., "Noise Suppressing Turbofan Nozzles and Method," US Patent 4288984, September 1981.

9. Majjigi, R. K., Brausch, J. F., Janardan, B. A., Balsa, T. F., Knott, P. R. and Pickup, N., "Free Jet Feasibility Study of a Thermal Acoustic Shield Concept for AST/VCE Application," NASA CR-3758, 1984.

10. Seiner, J. M. and Krejsa, E. A., "Supersonic Jet Noise and the High Speed Civil Transport," AIAA Paper 89-2358, July 1989.

11. Papamoschou, D., "Fan Flow Deflection in Simulated Turbofan Exhaust," AIAA Journal, Vol. 44, No. 12, 2006, pp. 3088-3097.

12. Papamoschou, D., "Pylon-Based Jet Noise Suppressors," AIAA Journal, Vol. 47, N0. 6, 2009, pp. 1408-1420.

13. Zaman, K. B. M. Q. and Papamoschou, D., "Effect of a Wedge on Coannular Jet Noise," AIAA Paper 2006-7, January 2006.

14. Zaman, K. B. M. Q., Bridges, J. E. and Papamoschou, D., "Offset Stream Technology – Comparison of Results from UCI and GRC Experiments," AIAA Paper 2007-438, January 2007.

15. Bridges, J. E. and Henderson, B., "QAT Jet Noise," presented at NASA Langley, June 2006.

16. Brown, C., Bridges, J. E. and Henderson, B., "Offset Stream Technology Test – Summary of Results," AIAA Paper 2007-3664, May 2007.

17. Viswanathan, K., "Nozzle Shaping for Reduction of Jet Noise from Single Jets," AIAA Journal, Vol. 43, Number 5, 2005, pp. 1008-1022.

18. Viswanathan, K., "An Elegant Concept for Reduction of Jet Noise from Turbofan Engines," Journal of Aircraft, Vol. 43, No. 3, May-June 2006, pp. 616-626.

19. Viswanathan, K., "Noise of Dual-Stream Beveled Nozzles at Supercritical Pressure Ratios," Journal of Aircraft, Vol. 43, No. 3, May-June 2006, pp. 627-638.

20. Viswanathan, K., Shur, M., Spalart, P. R. and Strelets, M., "Flow and Noise Predictions for Single and Dual-Stream Beveled Nozzles," AIAA Journal, Vol. 46, No. 3, March 2008, pp. 601-626.

21. Shur, M. L., Spalart, P. S., and Strelets, M., "Noise prediction for increasingly complex jets. Part I: Methods and Tests," International Journal of Aeroacoustics, Vol. 4, No. 3 and 4, 2005, pp. 213-246.

22. Shur, M. L., Spalart, P. S., and Strelets, M., "Noise prediction for increasingly complex jets. Part II: Applications," International Journal of Aeroacoustics, Vol. 4, No. 3 and 4, 2005, pp. 247-266.

23. Shur, M. L., Spalart, P. S., Strelets, M., and Garbaruk, A. V., "Further Steps in LES-Based Noise Prediction for Complex Jets," AIAA Paper 2006-485, January 2006.

24. Strelets, M. K., "Detached Eddy Simulation of Massively Separated Flows," AIAA Paper 2001-0879, January 2001.

25. Ffowcs Williams, J. E., and Hawkings, D. L., "Sound Generated by Turbulence and Surfaces in Unsteady Motion," Philosophical Transactions of the Royal Society, 1969, A264 (1151), 321-342.

26. Gulyaev, A. N., Kozlov, V. E., and Secundov, A. N., "A Universal One-Equation Model for Turbulent Viscosity," Fluid Dynamics, 28(4), 1991, pp. 484-494.

27. Shur, M., Strelets, M., Zaikov, L., Gulyaev, A., Kozlov, V., and Secundov, A., "Comparative Numerical Testing of One- and Two-Equation Turbulence Models for Flows with Separation and Reattachment," AIAA Paper-1995-0863, January 1995.

28. Viswanathan, K., "Jet Aeroacoustic Testing: Issues and Implications," AIAA Journal, Vol. 41, No. 9, 2003, pp. 1674-1689.

29. Viswanathan, K., "Instrumentation Considerations for Accurate Jet Noise Measurements," AIAA Journal, Vol. 44, No. 6, 2006, pp. 1137-1149.

30. Shields, F. D. and Bass, H. E., "Atmospheric Absorption of High Frequency Noise and Application to Fractional-Octave Band," NASA-CR 2760, 1977.

31. Amiet, R. K., "Correction of Open Jet Wind Tunnel Measurements for Shear Layer Refraction," AIAA paper 75-532, 1975.

32. Amiet, R. K., "Refraction of Sound by a Shear Layer," Journal of Sound and Vibration, 58(4), 1978, pp. 467-482.

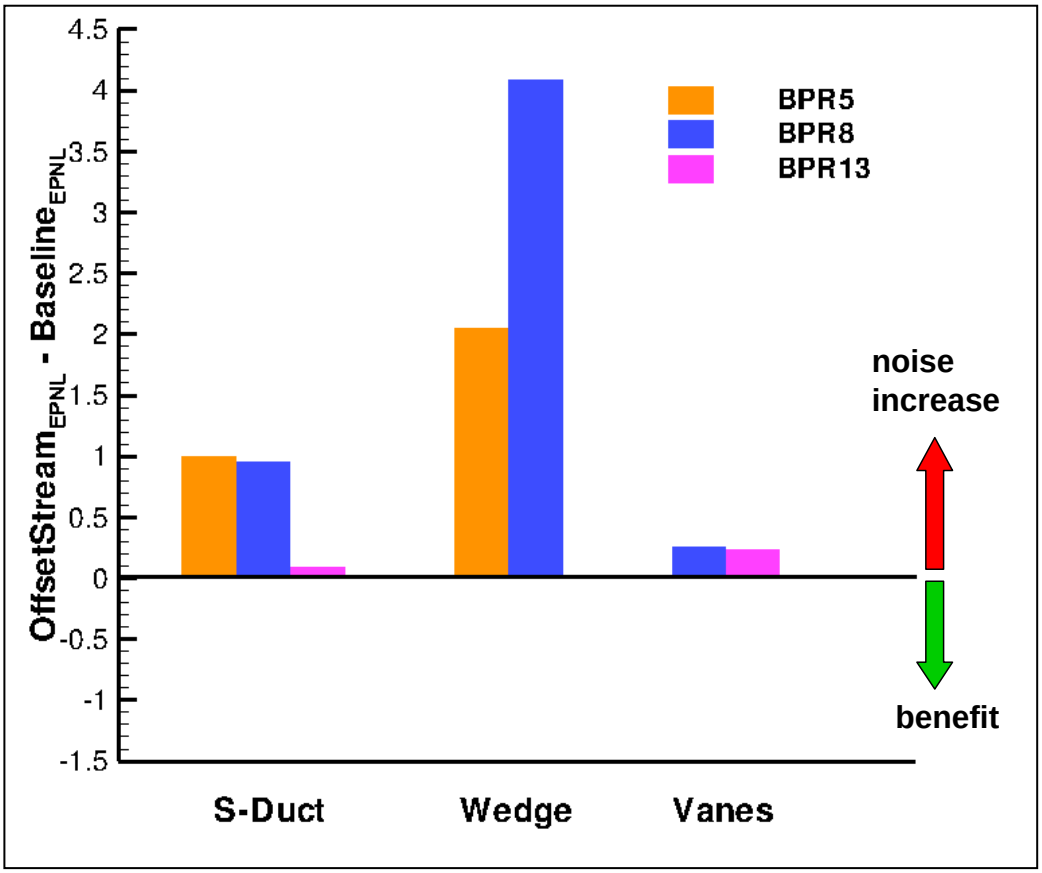

Figure 1. Effect of offset stream concepts on EPNL at typical takeoff power and various bypass ratios. $M_t = 0.20$. Reproduced from Ref. [16].

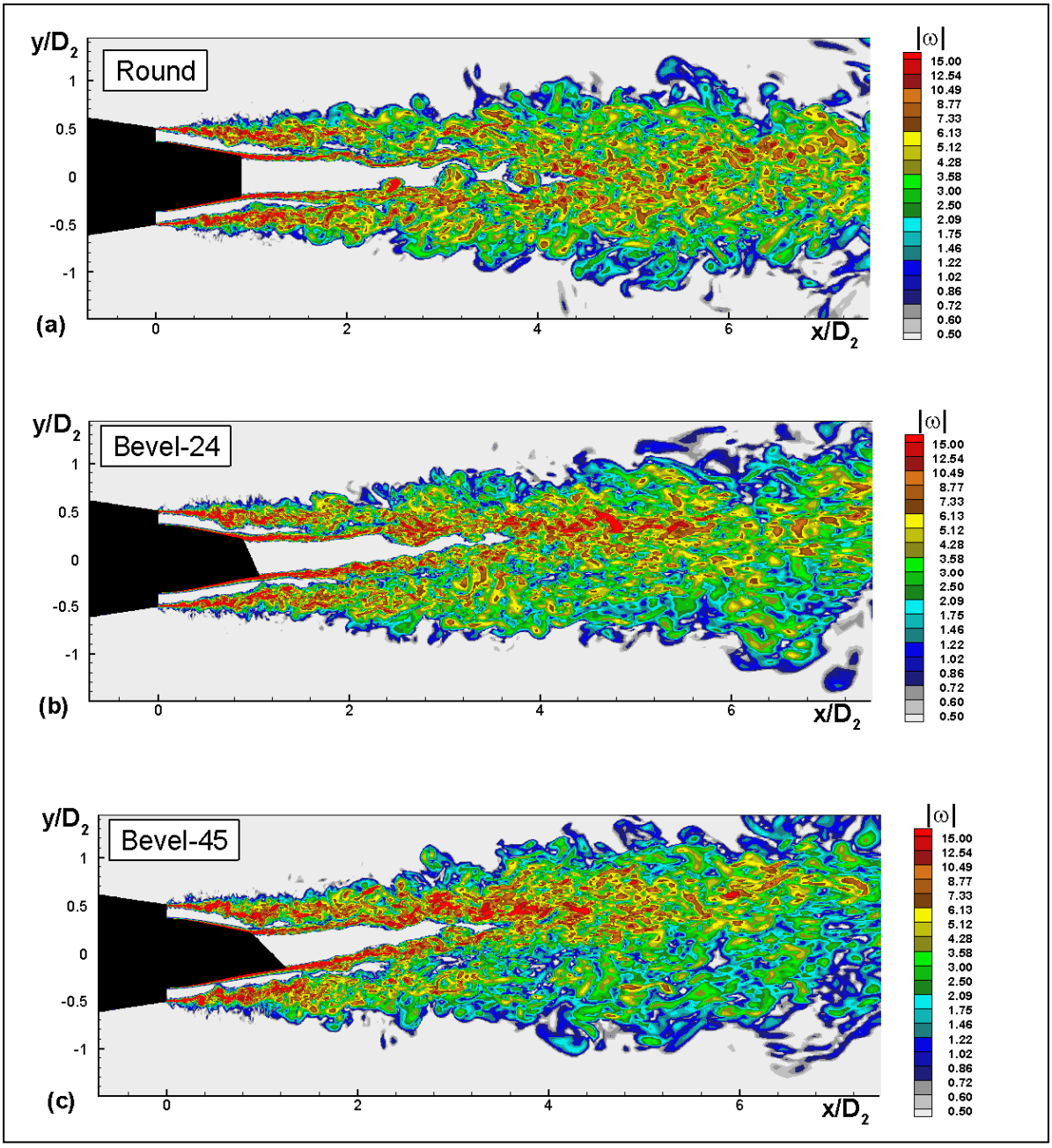

Figure 2. Effect of primary nozzle beveling on snapshots of vorticity for a dual-stream jet. NPR_p=NPR_s=1.8, T_p/T_a =2.37, T_s/T_a =1.0. (a) round; (b) bevel24; (c) bevel45.

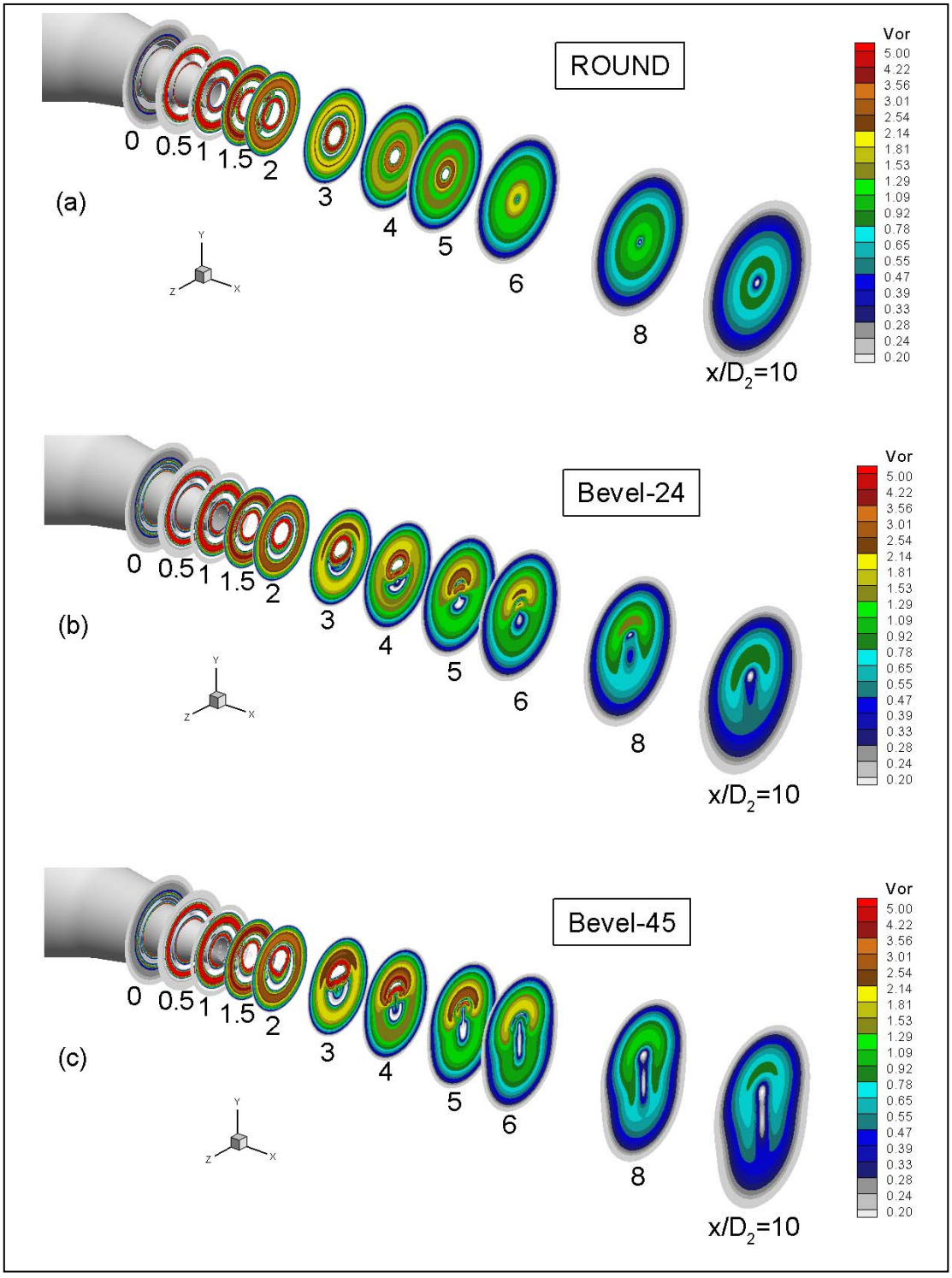

Figure 3. Vorticity contours for the dual-stream jets at various cross sections. NPR_p=NPR_s=1.8, T_p/T_a =2.37, T_s/T_a =1.0. (a) round; (b) bevel24; (c) bevel45.

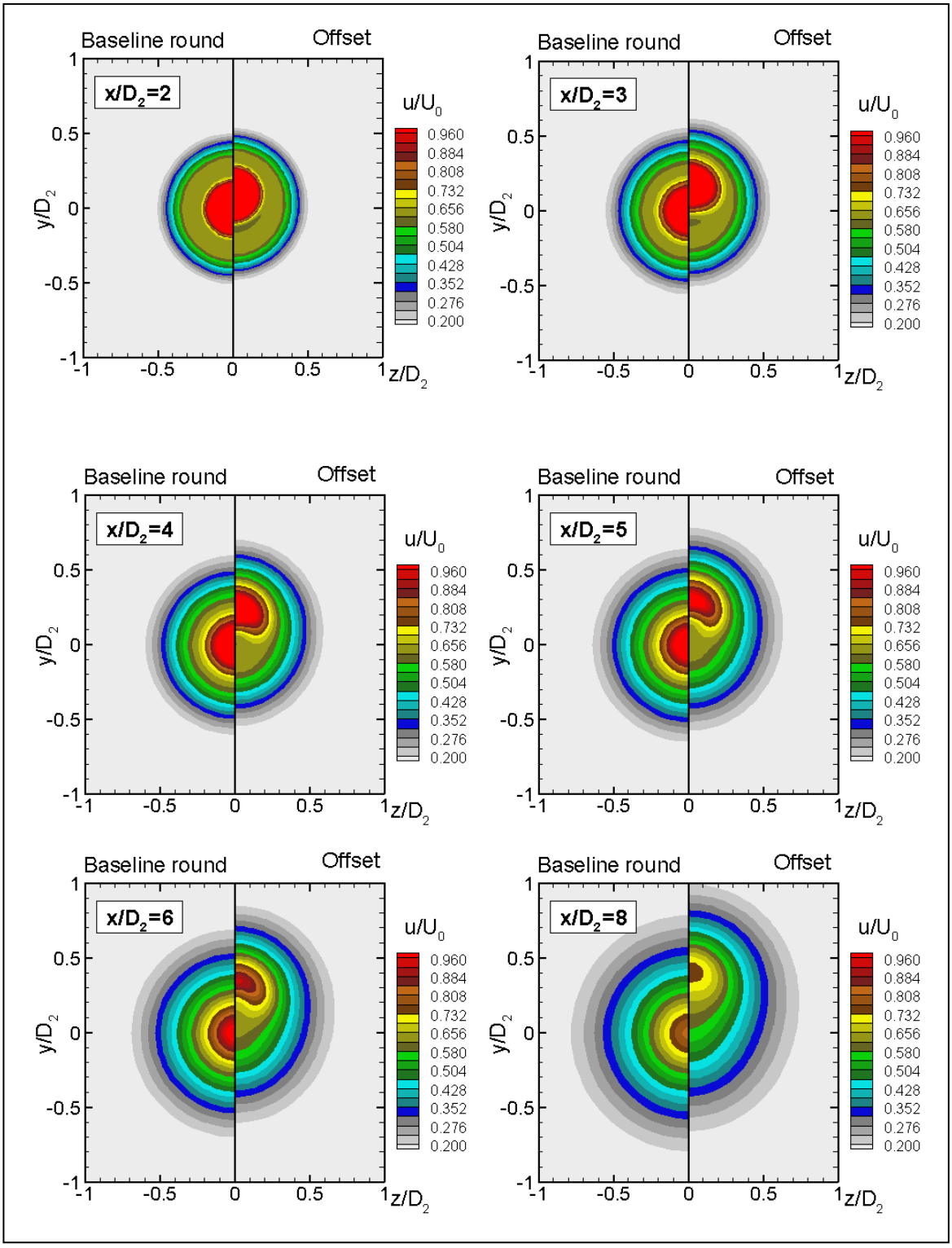

Figure 4. Streamwise velocity in cross-sectional plane. NPR_p=NPR_s=1.8, T_p/T_a=2.37, T_s/T_a=1.0 and M_t=0.20. Left: baseline (round + round); right: bevel24 + round.

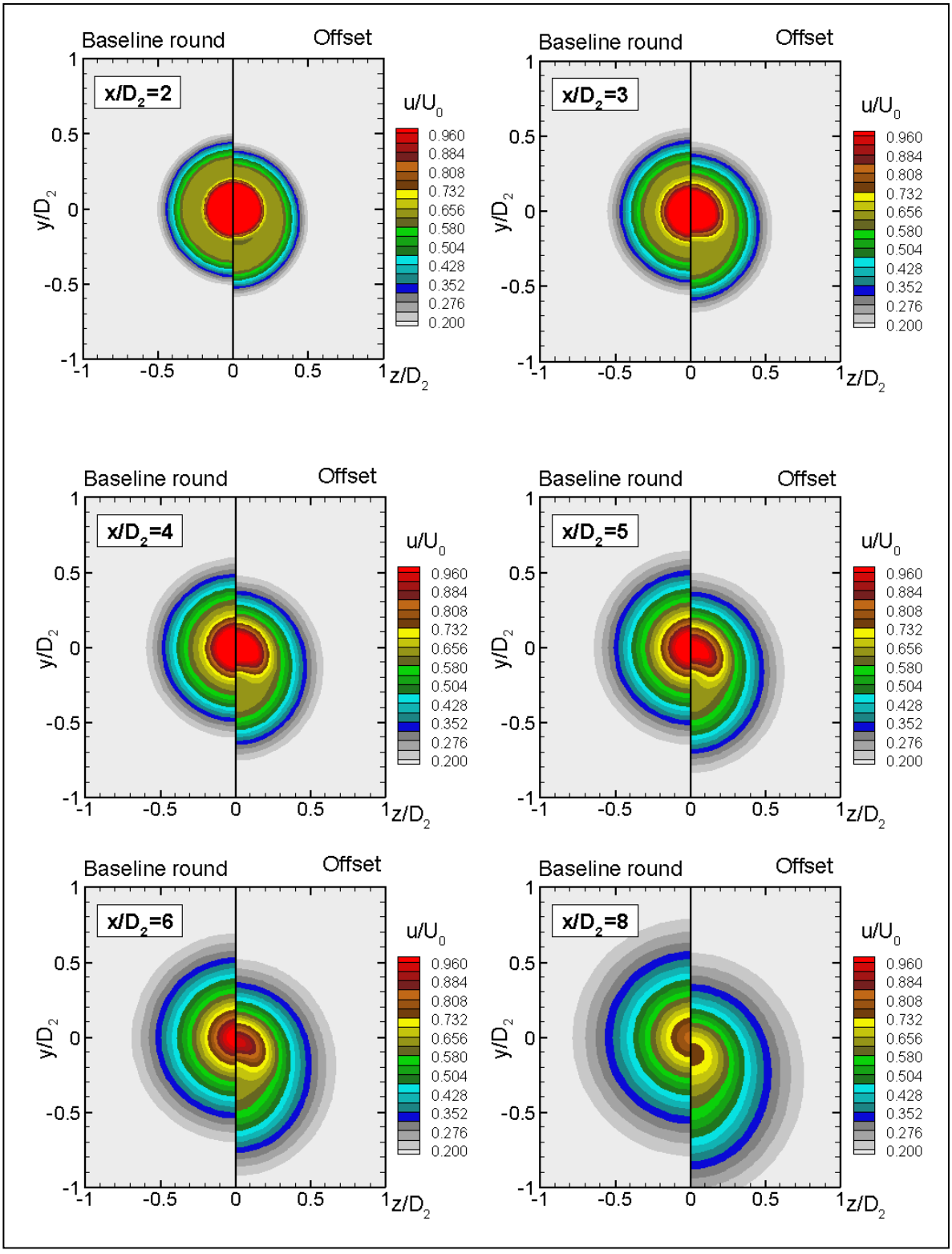

Figure 5. Streamwise velocity in cross-sectional plane. NPR_p=NPR_s=1.8, T_p/T_a=2.37, T_s/T_a=1.0 and M_t=0.20. Left: baseline (round + round); right: round + modified-A.

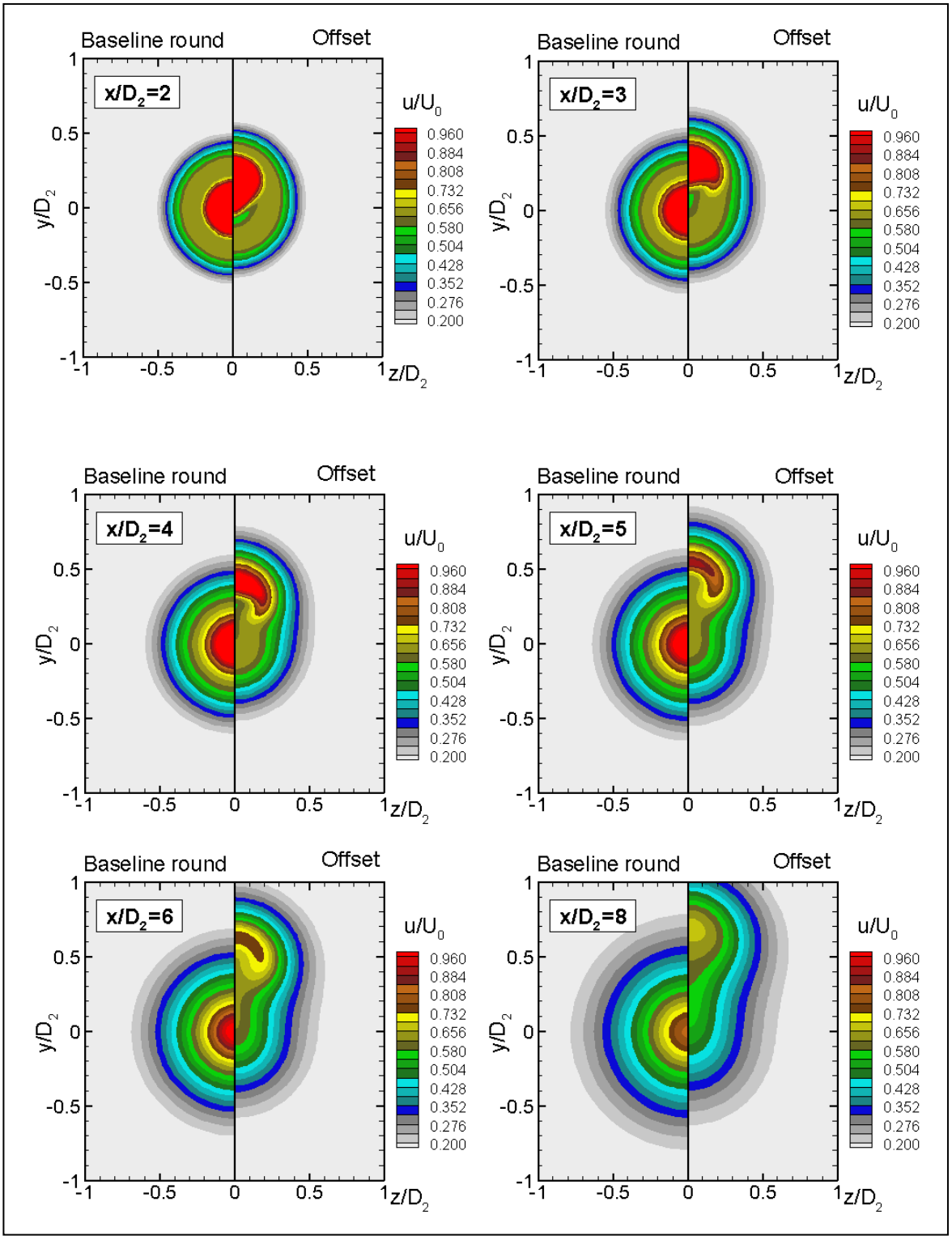

Figure 6. Streamwise velocity in cross-sectional plane. NPR_p=NPR_s=1.8, T_p/T_a=2.37, T_s/T_a=1.0 and M_t=0.20. Left: baseline (round + round); right: bevel45 + round.

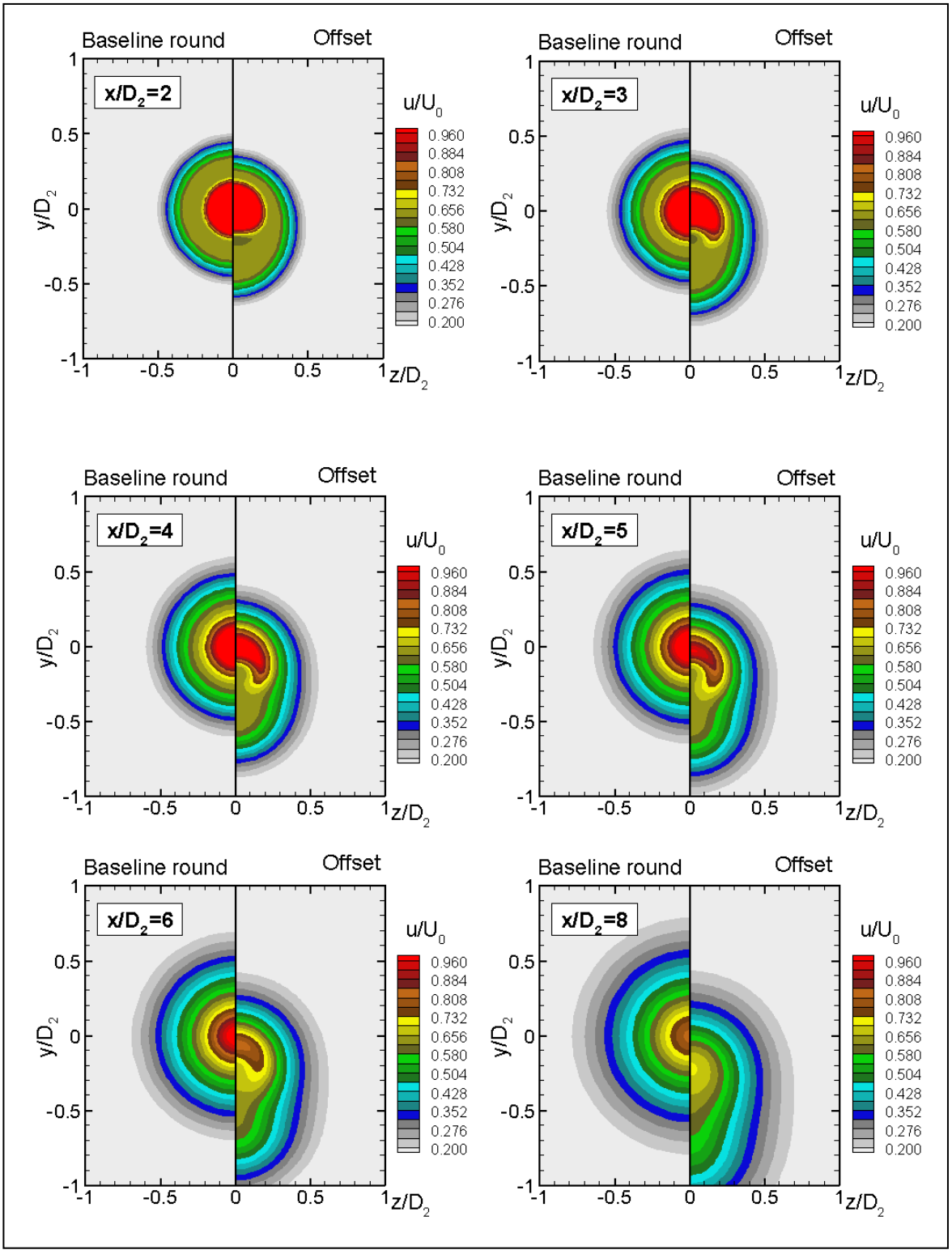

Figure 7. Streamwise velocity in cross-sectional plane. NPR_p=NPR_s=1.8, T_p/T_a=2.37, T_s/T_a=1.0 and M_t=0.20. Left: baseline (round + round); right: round + modified-B.

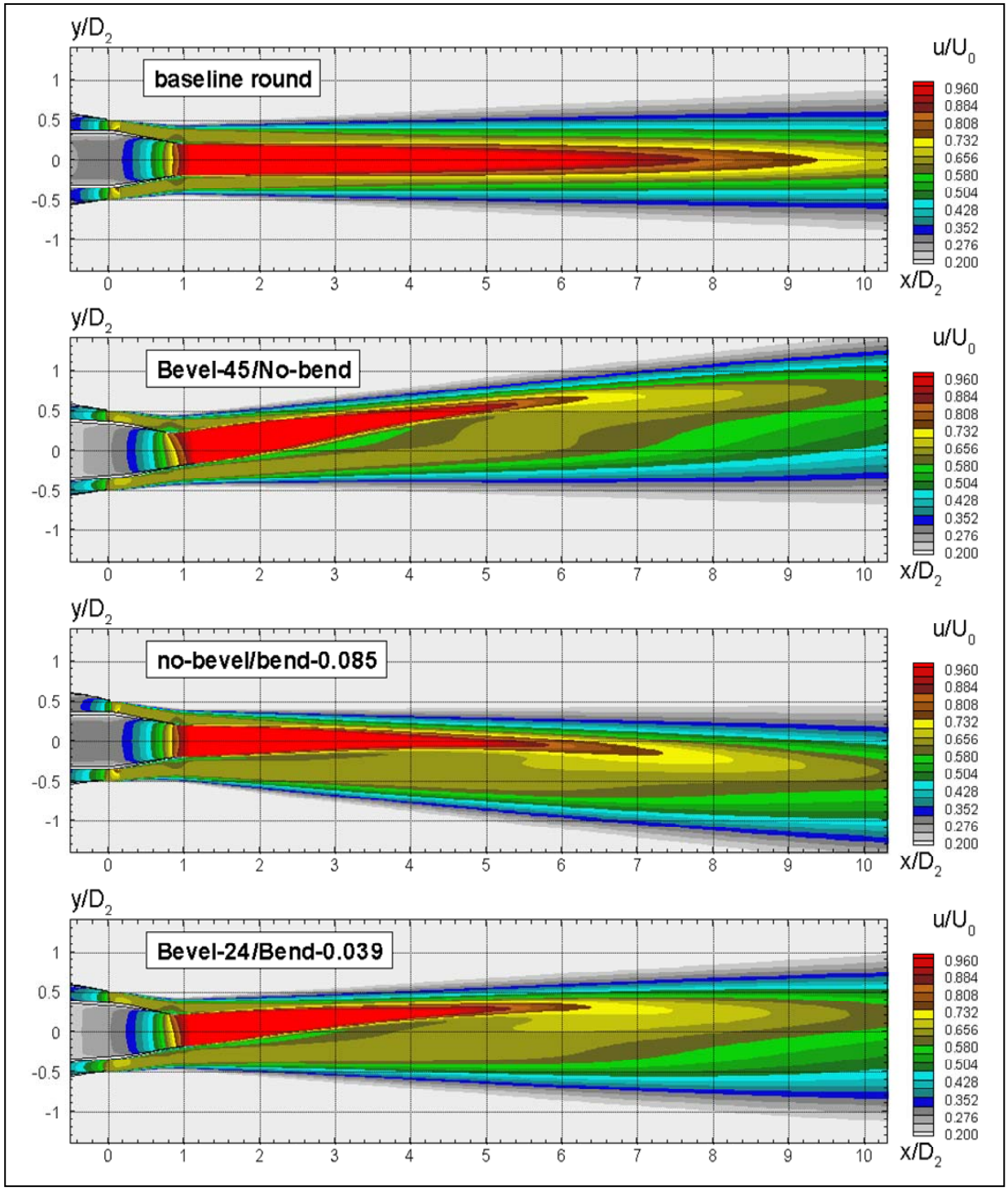

Figure 8. Axial variation of streamwise velocity in symmetry plane of jet. NPR_p=NPR_s=1.8, T_p/T_a=2.37, T_s/T_a=1.0 and M_t=0.20. a) baseline; b) bevel45 + round; c) round + modified-B; d): bevel24 + modified-C.

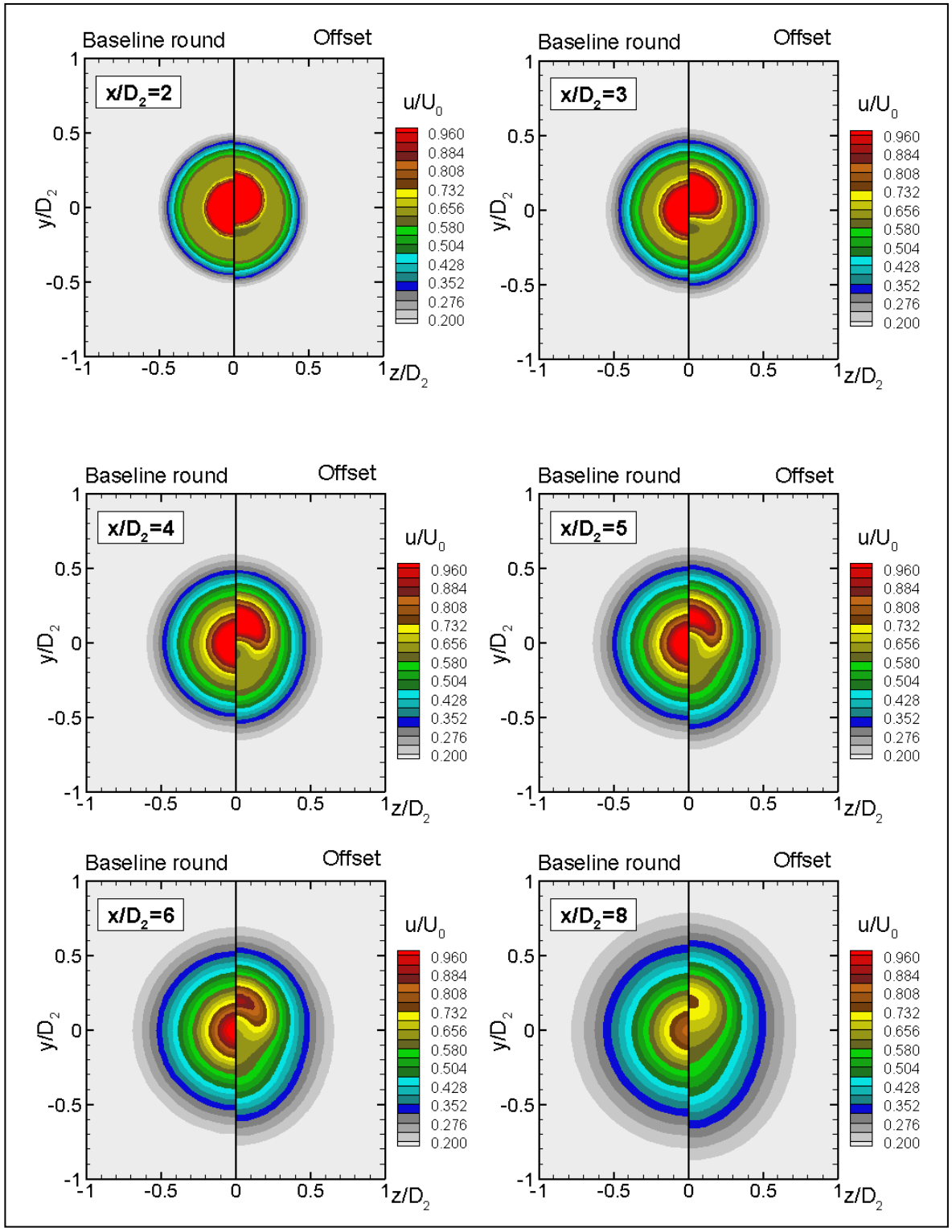

Figure 9. Streamwise velocity in cross-sectional plane. NPR_p=NPR_s=1.8, T_p/T_a=2.37, T_s/T_a=1.0 and M_t=0.20. Left: baseline (round + round); right: bevel15 + modified-D.

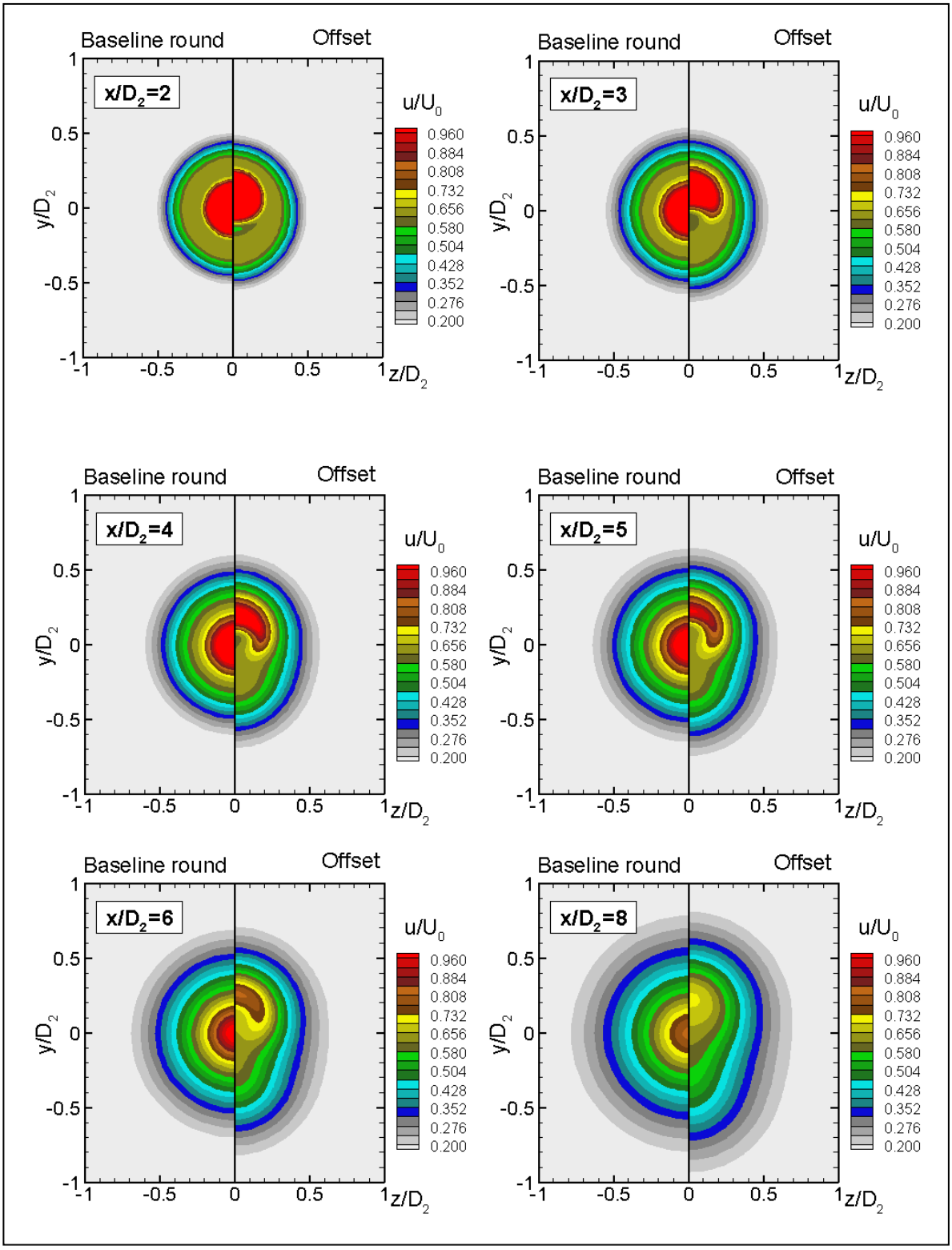

Figure 10. Streamwise velocity in cross-sectional plane. NPR_p=NPR_s=1.8, T_p/T_a=2.37, T_s/T_a=1.0 and M_t=0.20. Left: baseline (round + round); right: bevel20 + modified-E.

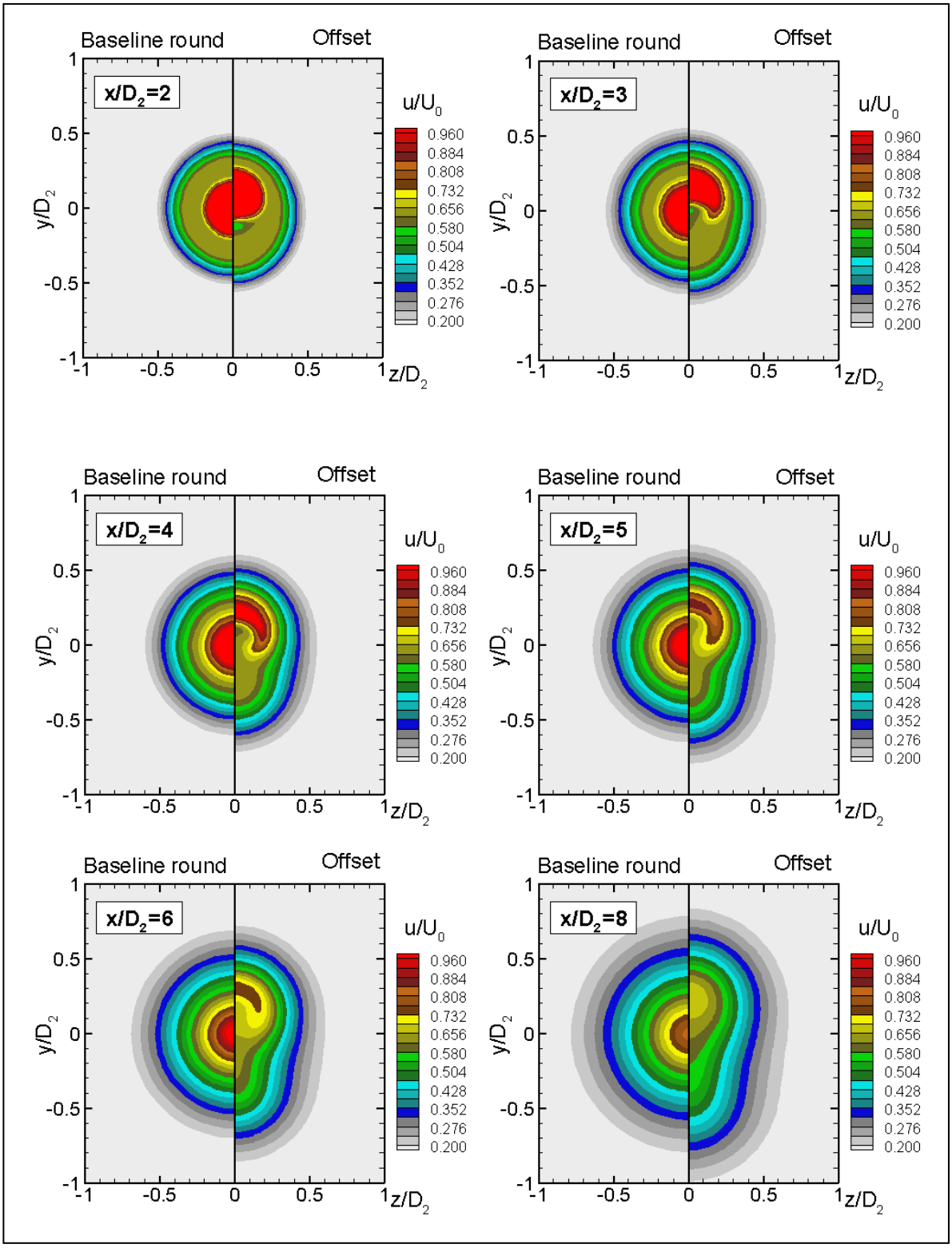

Figure 11. Streamwise velocity in cross-sectional plane. NPR_p=NPR_s=1.8, T_p/T_a=2.37, T_s/T_a=1.0 and M_t=0.20. Left: baseline (round + round); right: bevel24 + modified-C.

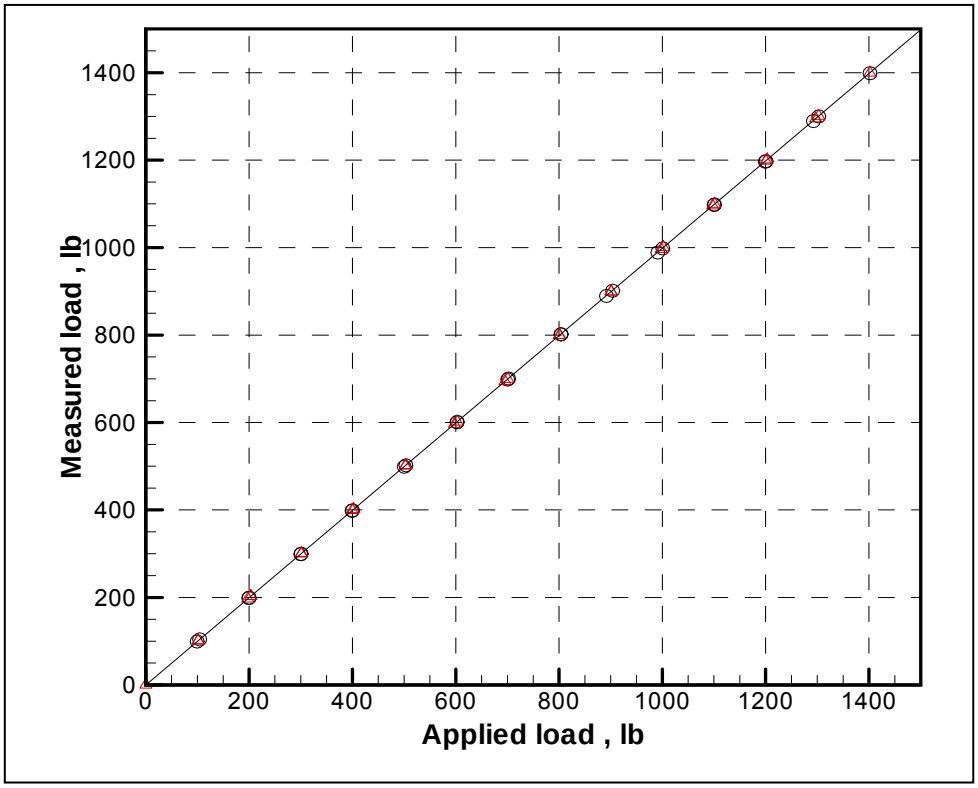

Figure 12. Calibration of force balance showing measured load versus applied load. o: pre-test; Δ: post test.

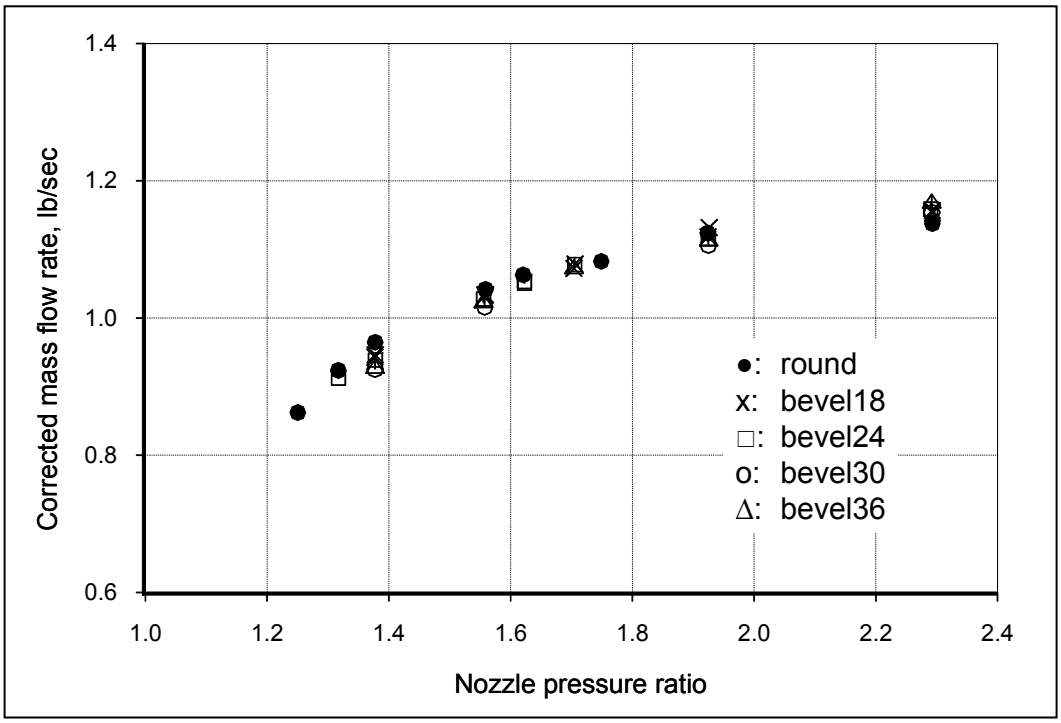

Figure 13. Comparison of corrected mass flow rates for the baseline and beveled nozzles.

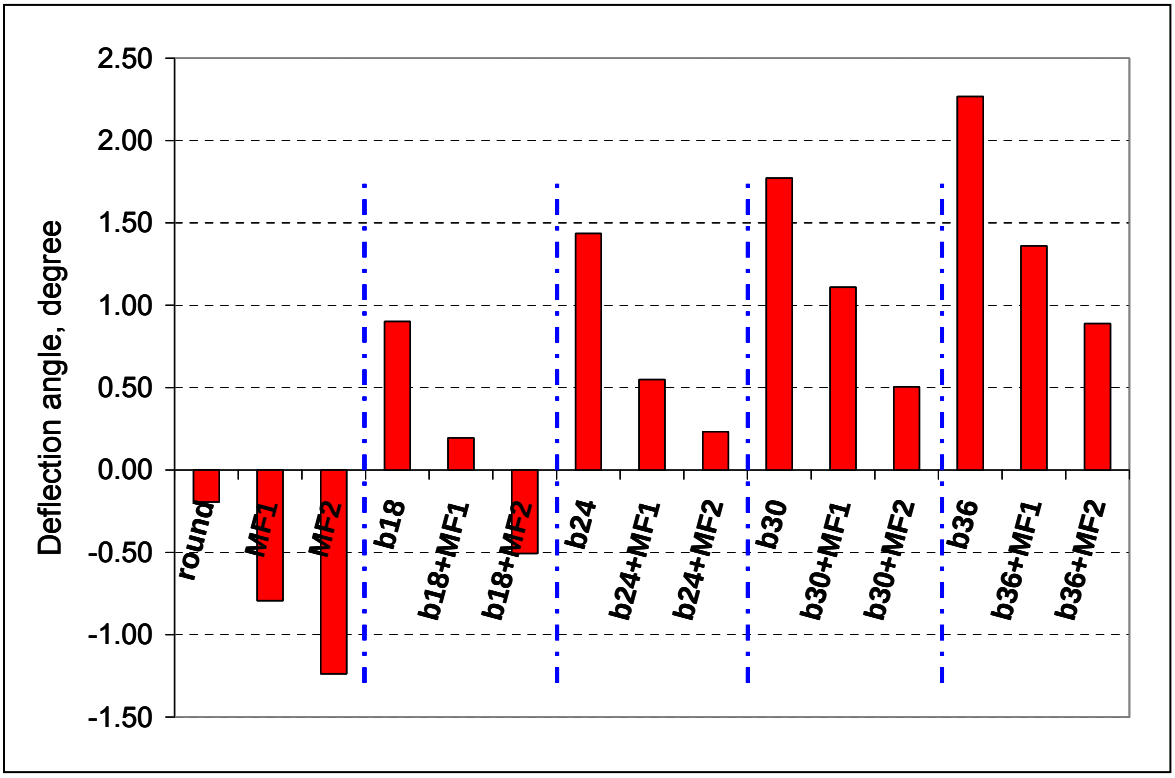

Figure 14. Plume deflection angle for different nozzle geometries. NPR_p=1.71, T_p/T_a=3.16, NPR_s=1.76, T_s/T_a=1.24.

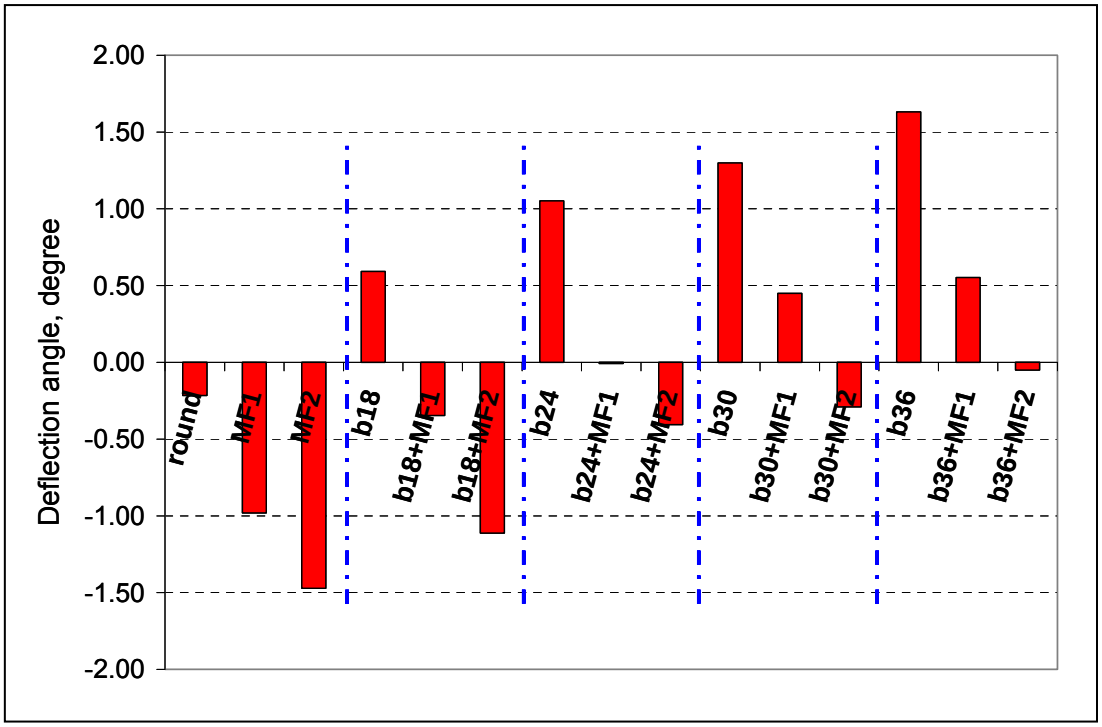

Figure 15. Plume deflection angle for different nozzle geometries. NPR_p=1.38, T_p/T_a=2.74, NPR_s=1.56, T_s/T_a=1.16.

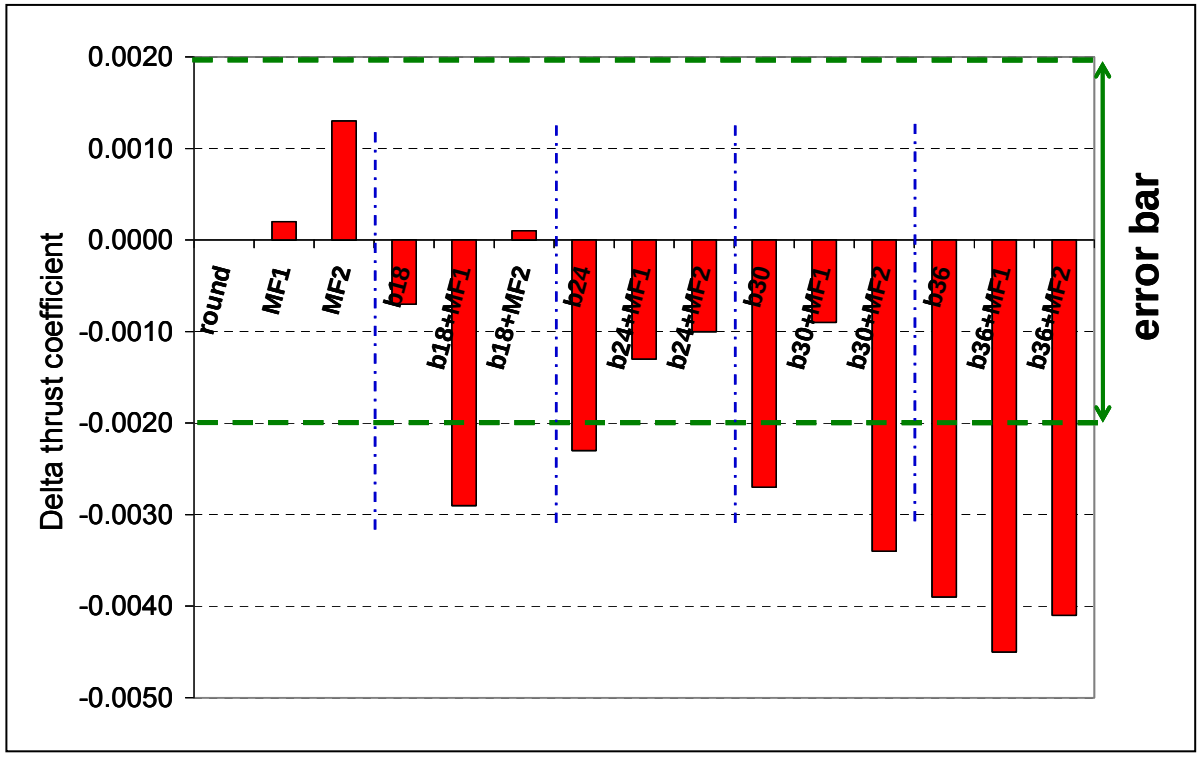

Figure 16. Difference in thrust performance relative to baseline nozzle geometry. NPR_p=1.71, T_p/T_a=3.16, NPR_s=1.76, T_s/T_a=1.24.

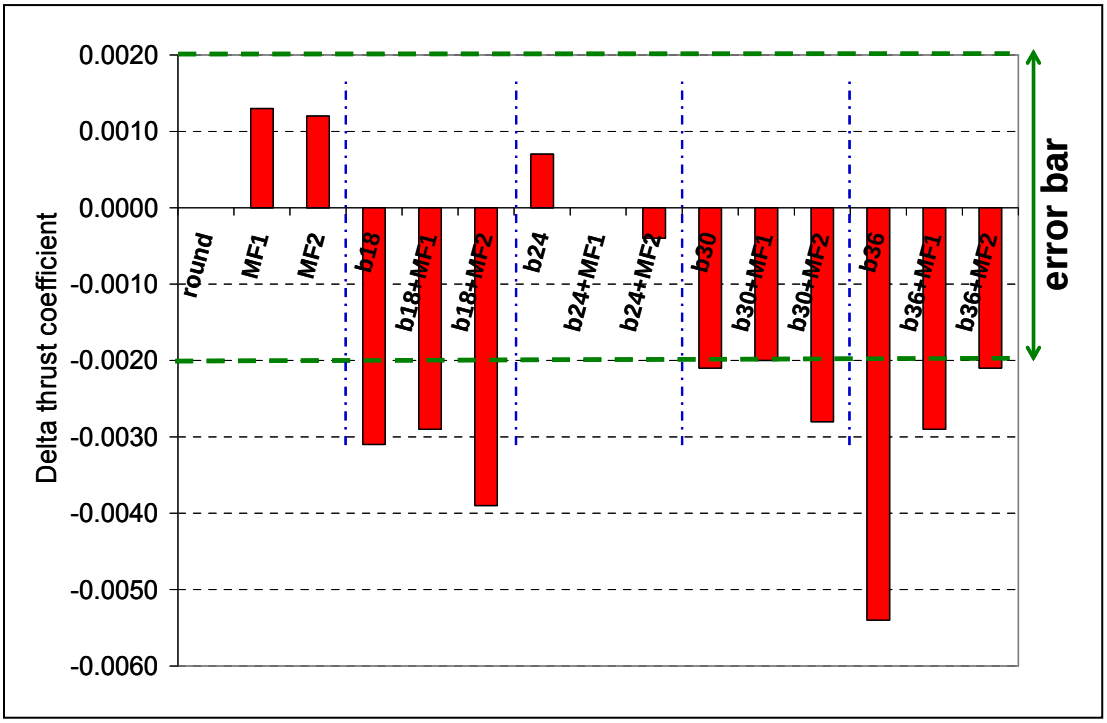

Figure 17. Difference in thrust performance relative to baseline nozzle geometry. NPR_p=1.38, T_p/T_a=2.74, NPR_s=1.56, T_s/T_a=1.16.

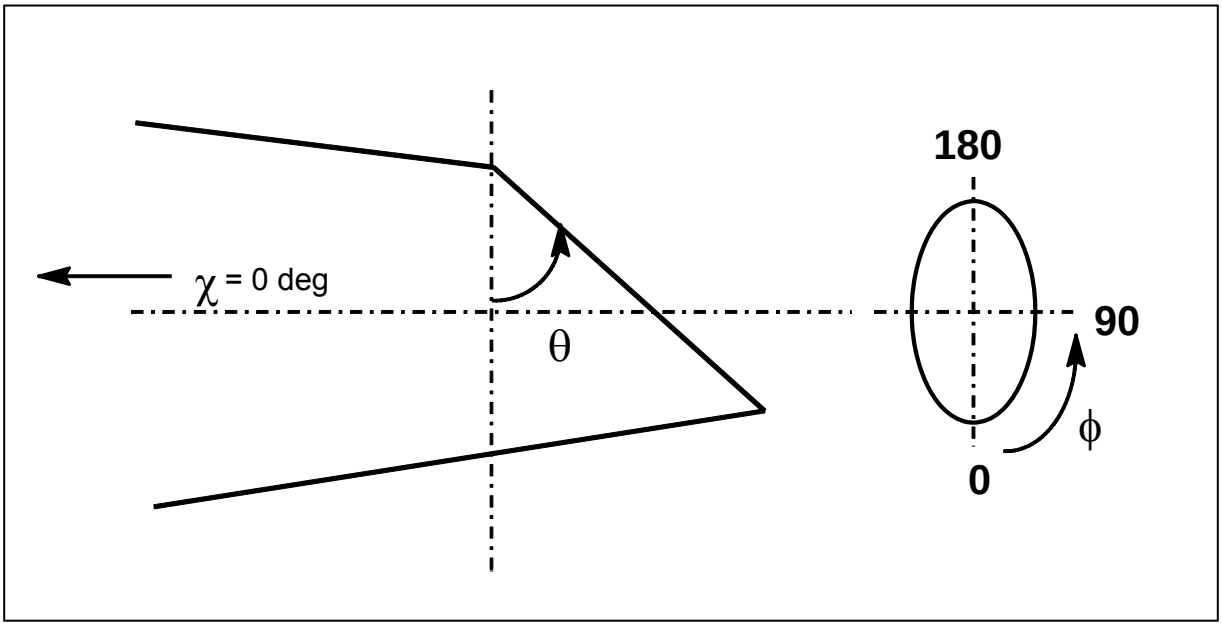

Figure 18. Conceptual sketch of the beveled nozzle and the measurement convention for the bevel angle (θ), the polar angle (χ) and the azimuthal angle (ϕ)

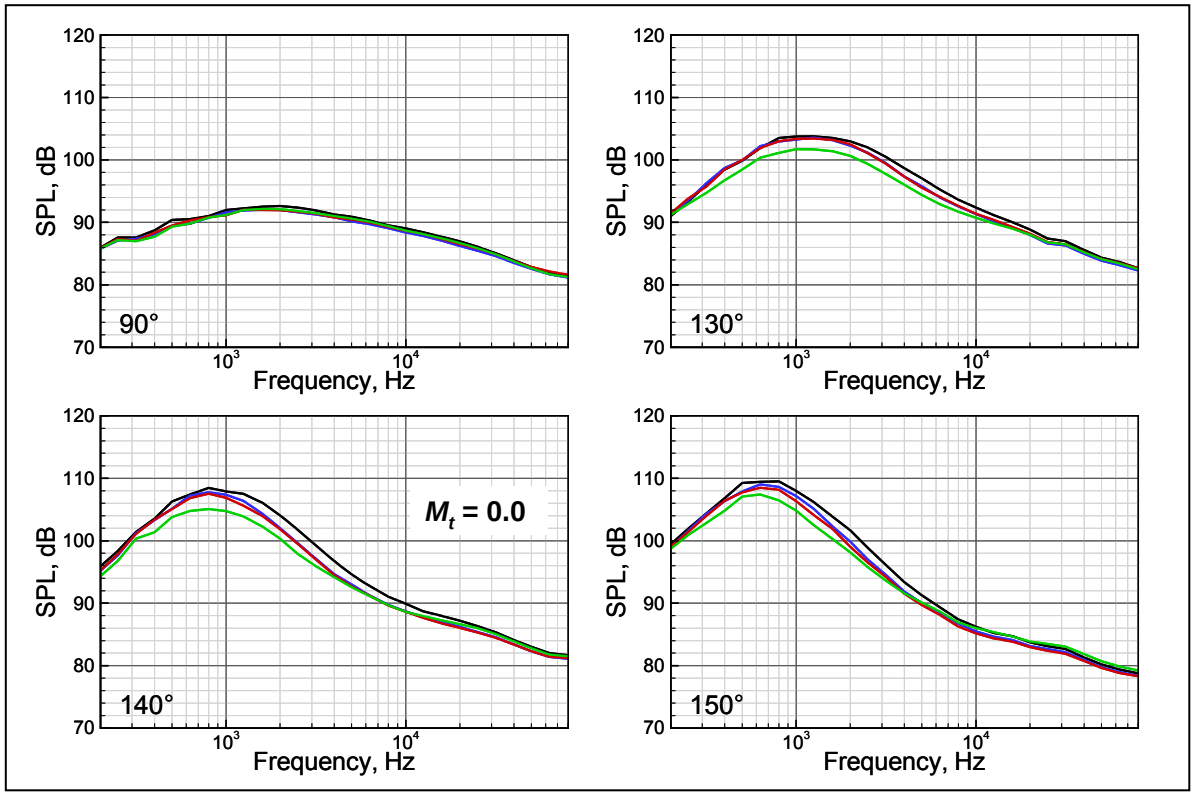

Figure 19. Spectral changes due to nozzle modifications. NPR_p=1.55, T_p/T_a=3.0, NPR_s=1.71, T_s/T_a=1.21. Black: baseline; blue: round+MF1; red: round+MF2; green: bev24+round. ϕ = 0°.

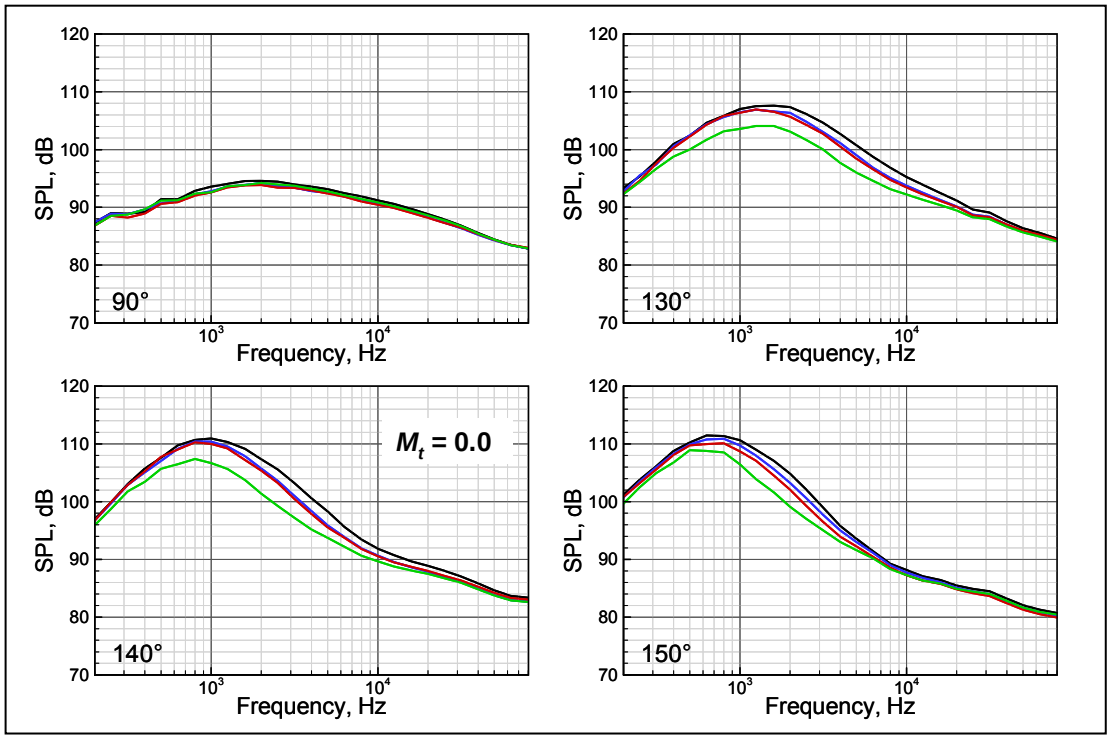

Figure 20. Spectral changes due to nozzle modifications. NPR_p=1.71, T_p/T_a=3.16, NPR_s=1.76, T_s/T_a=1.24. Black: baseline; blue: round+MF1; red: round+MF2; green: bev24+round. ϕ = 0°.

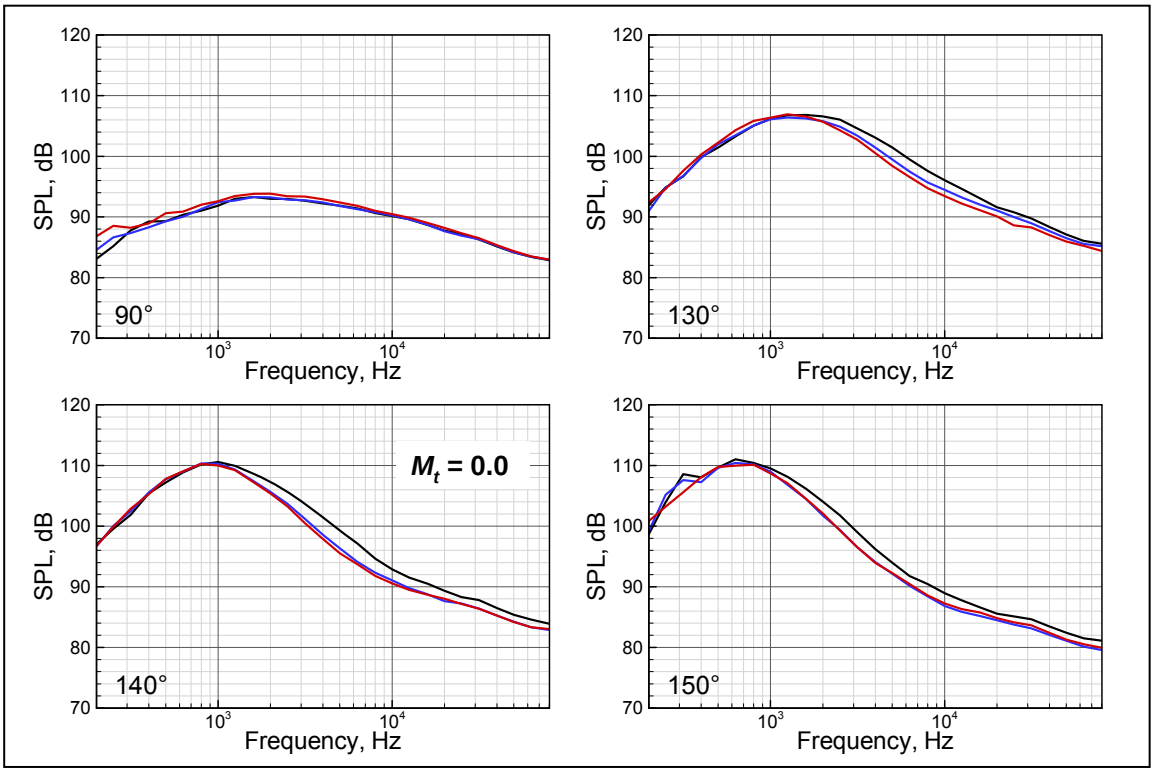

Figure 21. Azimuthal variation. NPR_p=1.71, T_p/T_a=3.16, NPR_s=1.76, T_s/T_a=1.24. Round + MF2. Black: ϕ = 60°; blue: ϕ = 30°; red: ϕ = 0°.

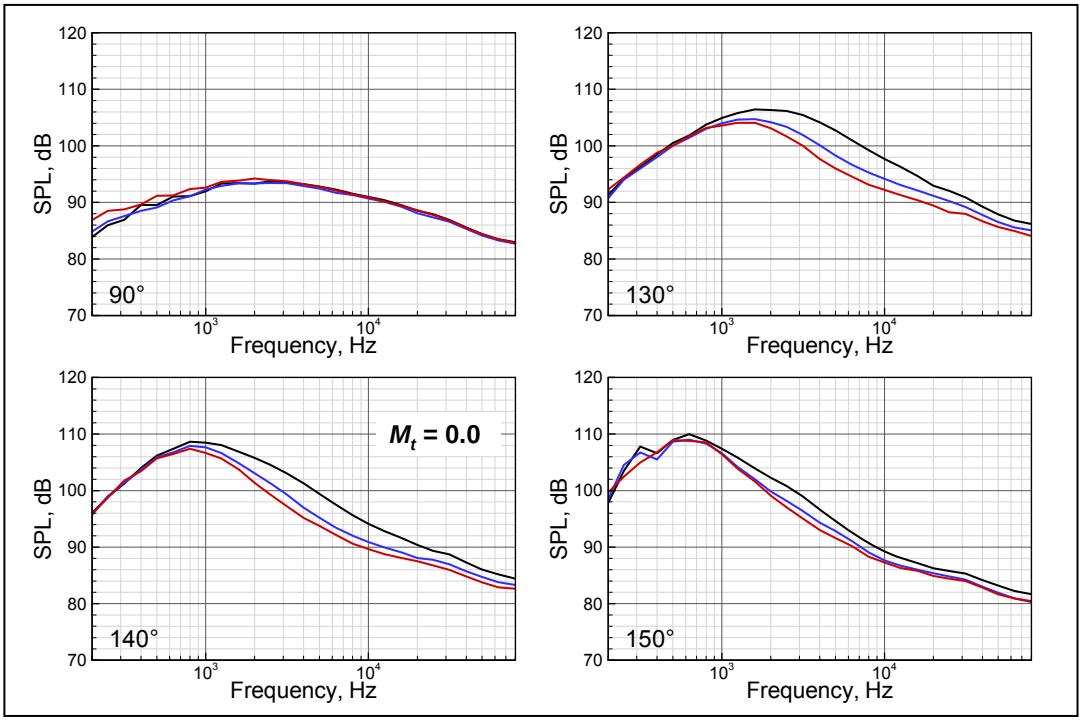

Figure 22. Azimuthal variation. NPR_p=1.71, T_p/T_a=3.16, NPR_s=1.76, T_s/T_a=1.24. Bevel24 + Round. Black: $\phi = 60°$; blue: $\phi = 30°$; red: $\phi = 0°$.

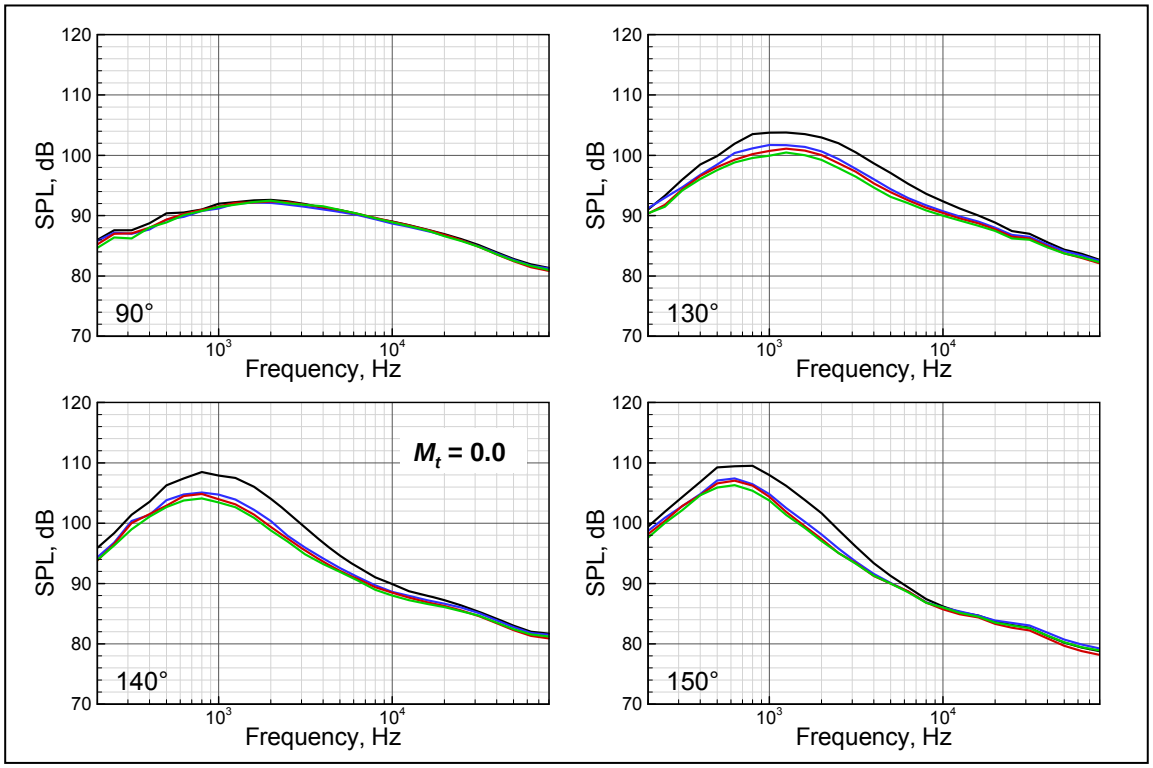

Figure 23. Spectral changes due to nozzle modifications. NPR_p=1.55, T_p/T_a=3.0, NPR_s=1.71, T_s/T_a=1.21. Black: baseline; blue: bev24+round; red: bev30+round; green: bev36+round. $\phi = 0°$.

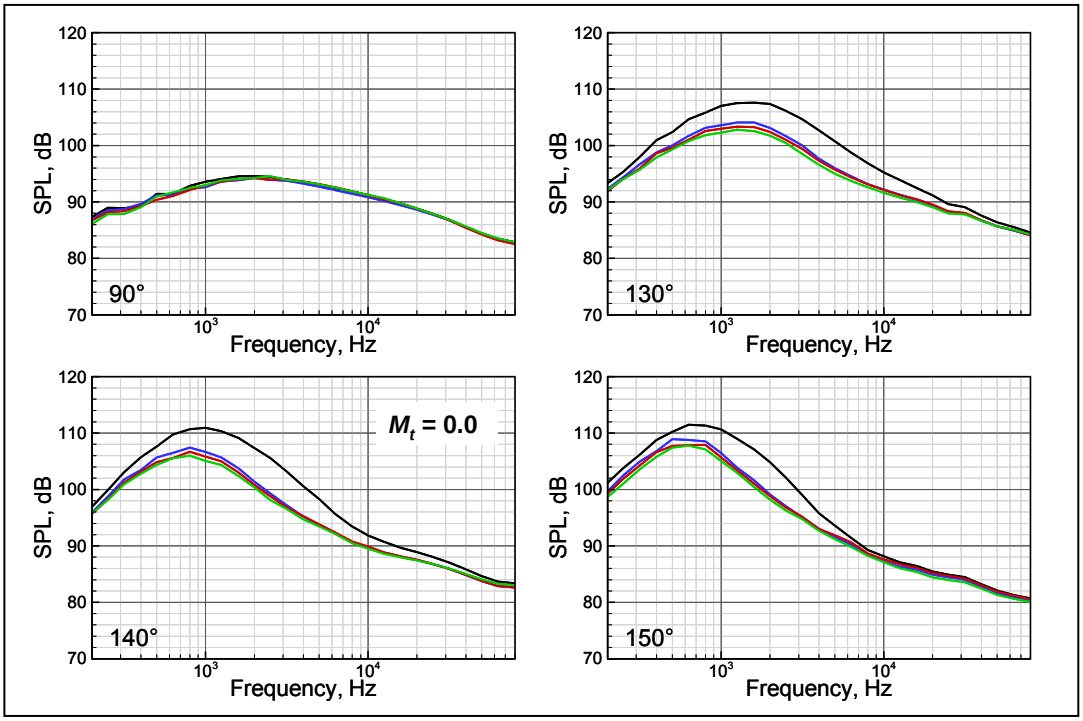

Figure 24. Spectral changes due to nozzle modifications. NPR_p=1.71, T_p/T_a=3.16, NPR_s=1.76, T_s/T_a=1.24. Black: baseline; blue: bev24+round; red: bev30+round; green: bev36+round. $\phi = 0°$.

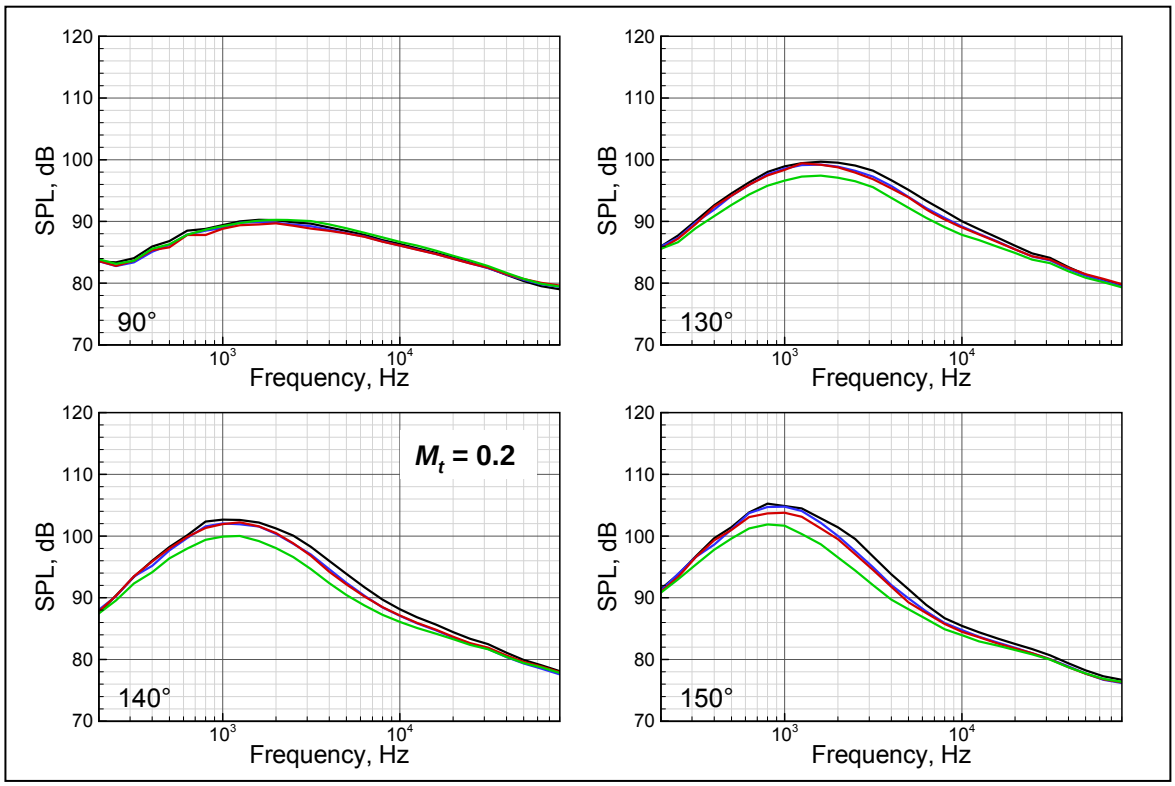

Figure 25. Spectral changes due to nozzle modifications. NPR_p=1.62, T_p/T_a=3.07, NPR_s=1.74, T_s/T_a=1.22. Black: baseline; blue: round+MF1; red: round+MF2; green: bev24+round. $\phi = 0°$.

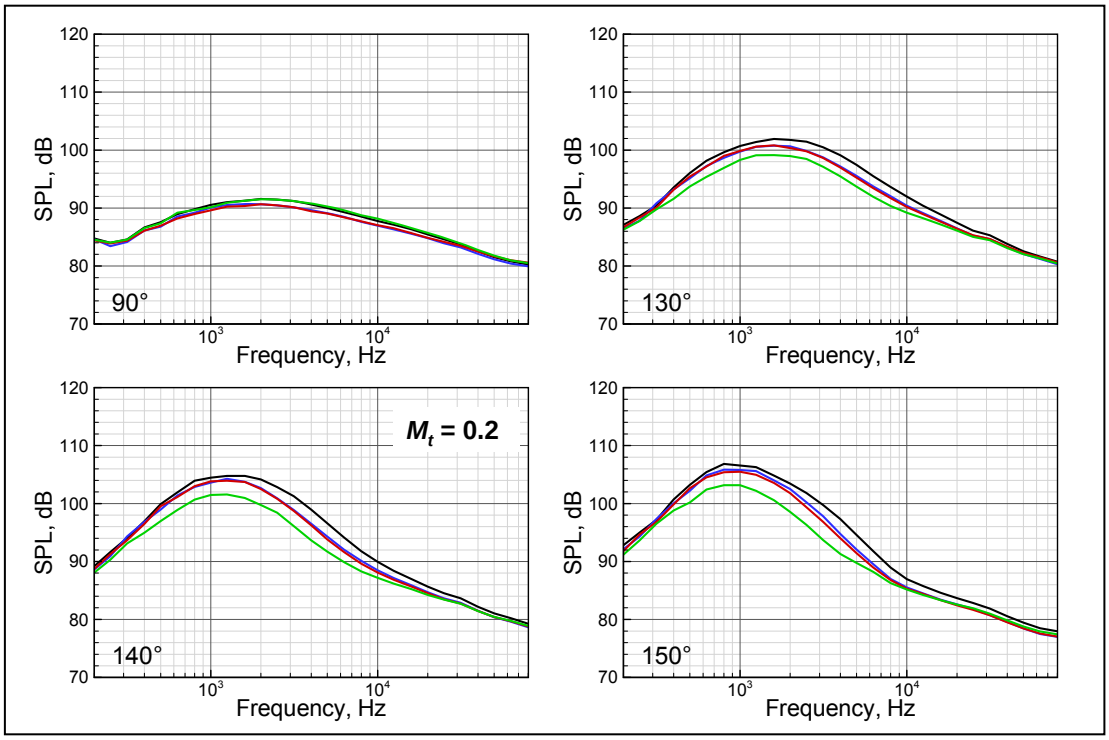

Figure 26. Spectral changes due to nozzle modifications. NPR_p=1.71, T_p/T_a=3.16, NPR_s=1.76, T_s/T_a=1.24. Black: baseline; blue: round+MF1; red: round+MF2; green: bev24+round. $\phi = 0°$.

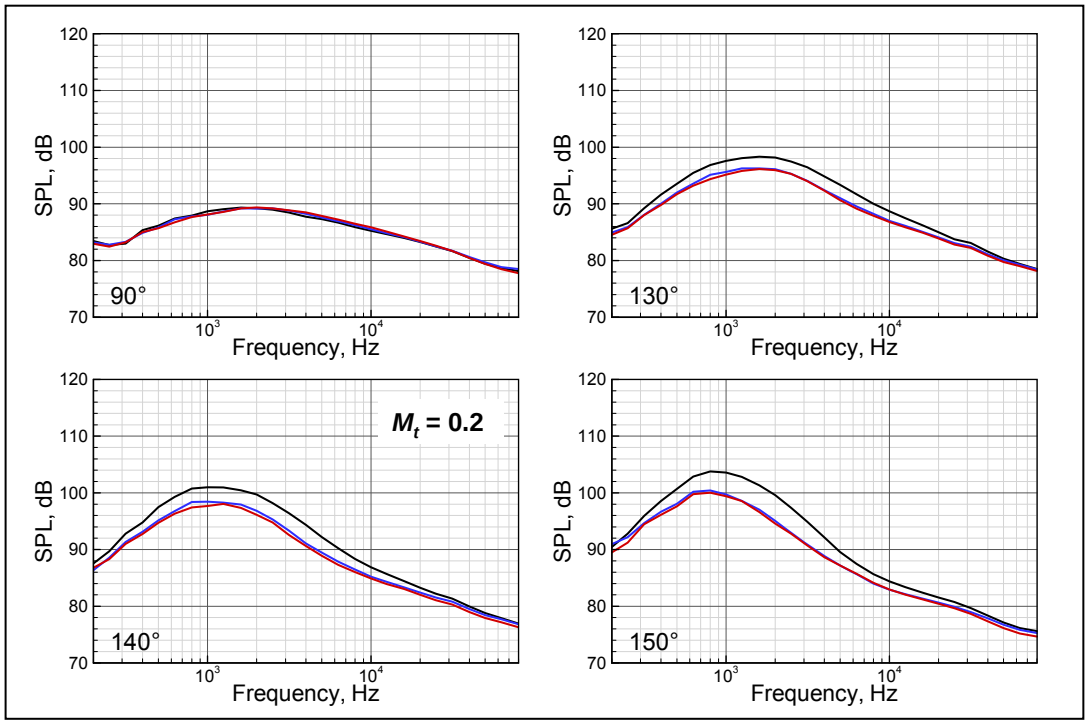

Figure 27. Spectral changes due to nozzle modifications. NPR_p=1.55, T_p/T_a=3.0, NPR_s=1.71, T_s/T_a=1.21. Black: baseline; blue: bevel24+round; red: bevel24+MF1. $\phi = 0°$.

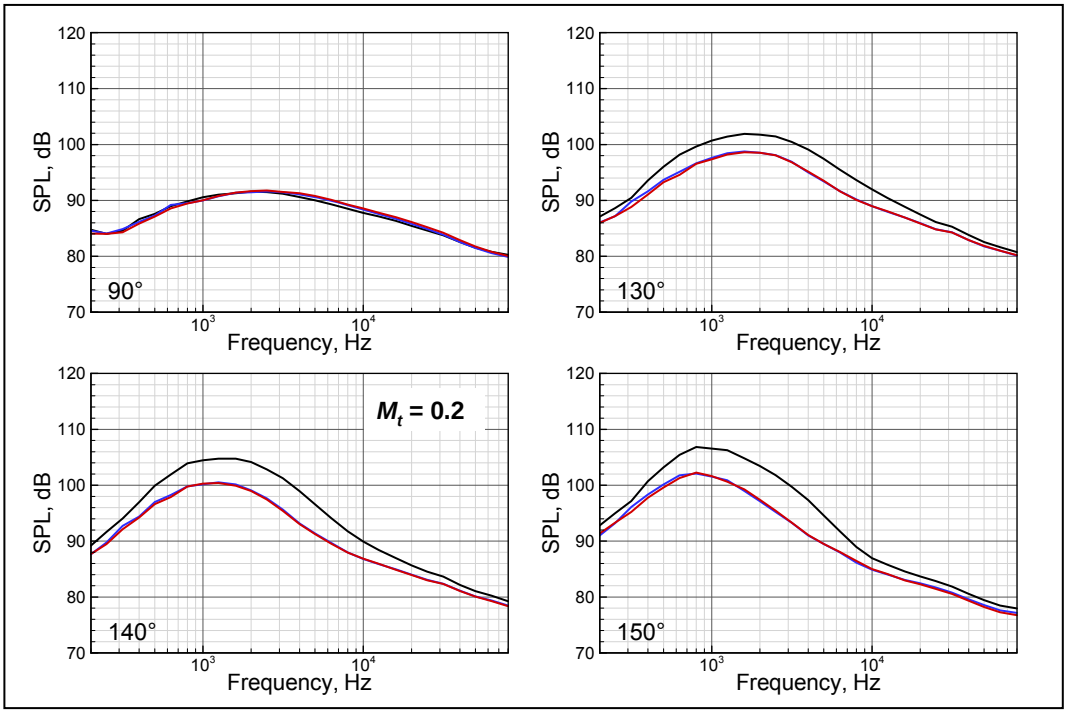

Figure 28. Spectral changes due to nozzle modifications. NPR_p=1.71, T_p/T_a=3.16, NPR_s=1.76, T_s/T_a=1.24. Black: baseline; blue: bevel30+round; red: bevel30+MF1. ϕ = 0°.

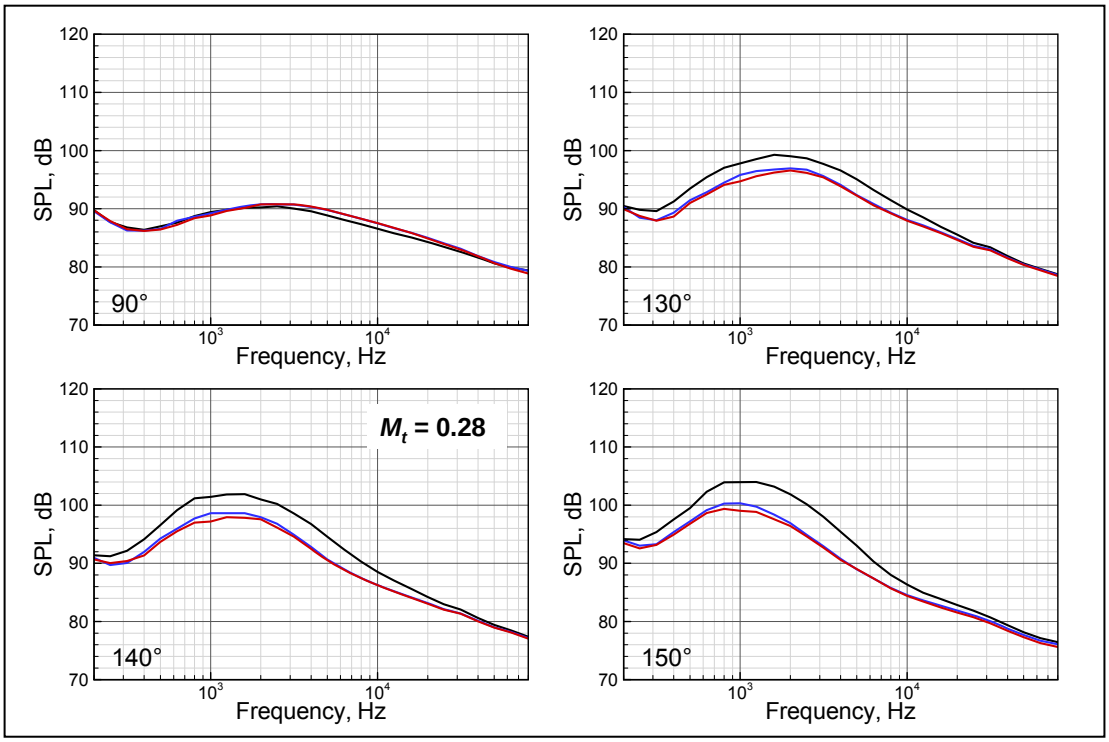

Figure 29. Spectral changes due to nozzle modifications. NPR_p=1.71, T_p/T_a=3.16, NPR_s=1.76, T_s/T_a=1.24. Black: baseline; blue: bevel30+round; red: bevel30+MF1. ϕ = 0°.

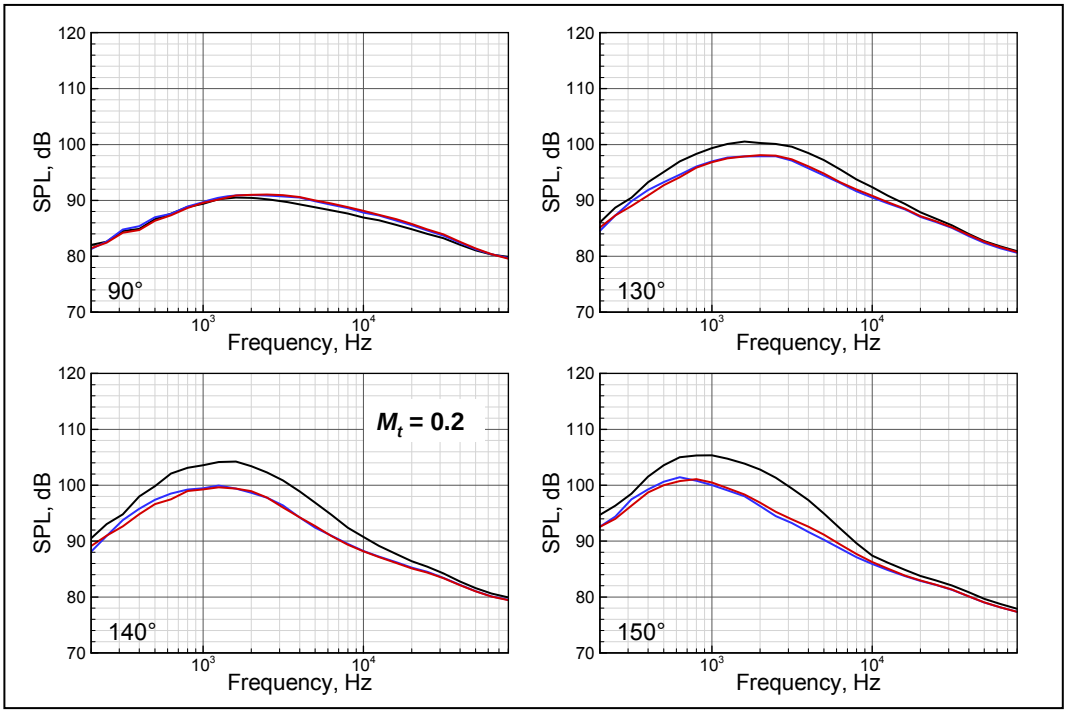

Figure 30. Spectral changes due to nozzle modifications. NPR_p=1.71, T_p/T_a=3.16, NPR_s=1.76, T_s/T_a=1.24. Black: baseline; blue: bevel30+round; red: bevel30+MF1. ϕ = 30°.

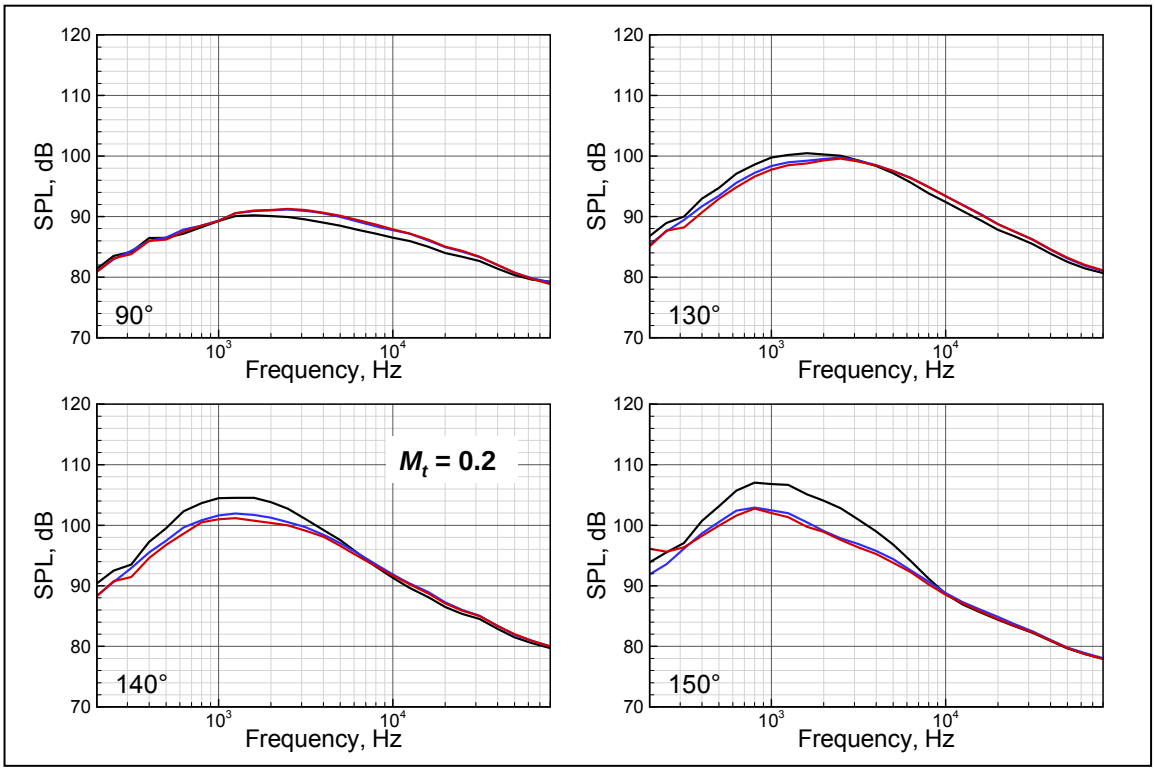

Figure 31. Spectral changes due to nozzle modifications. NPR_p=1.71, T_p/T_a=3.16, NPR_s=1.76, T_s/T_a=1.24. Black: baseline; blue: bevel30+round; red: bevel30+MF1. ϕ = 60°.

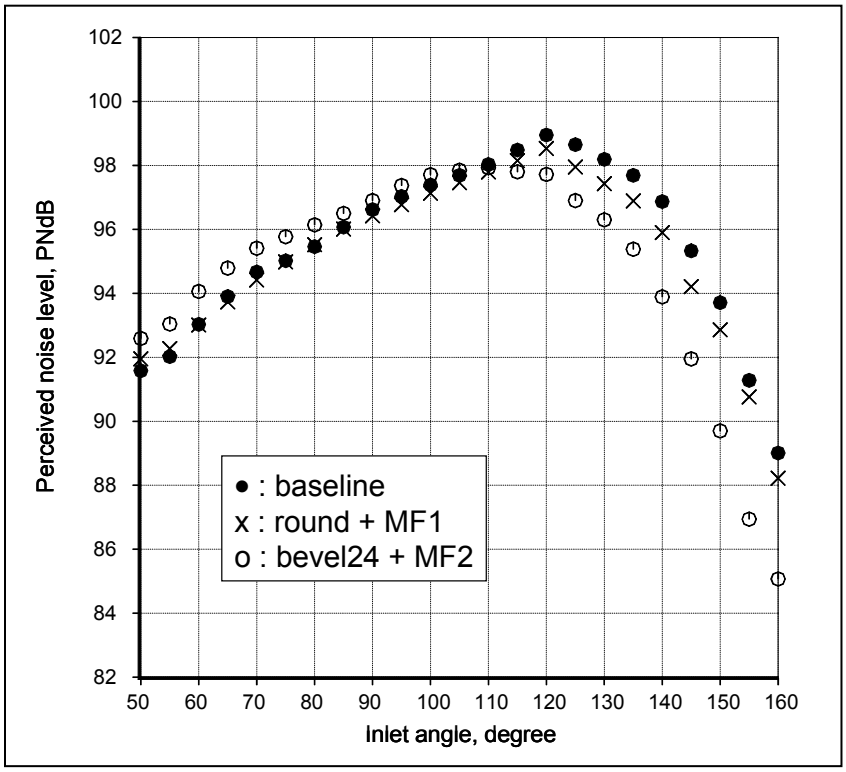

Figure 32. Variation of Perceived Noise Level with angle. NPR_p=1.62, T_p/T_a=3.07, NPR_s=1.74, T_s/T_a=1.22. •: baseline; x: round+MF1; o: bev24+MF2. $\phi = 0°$. M_t=0.20.

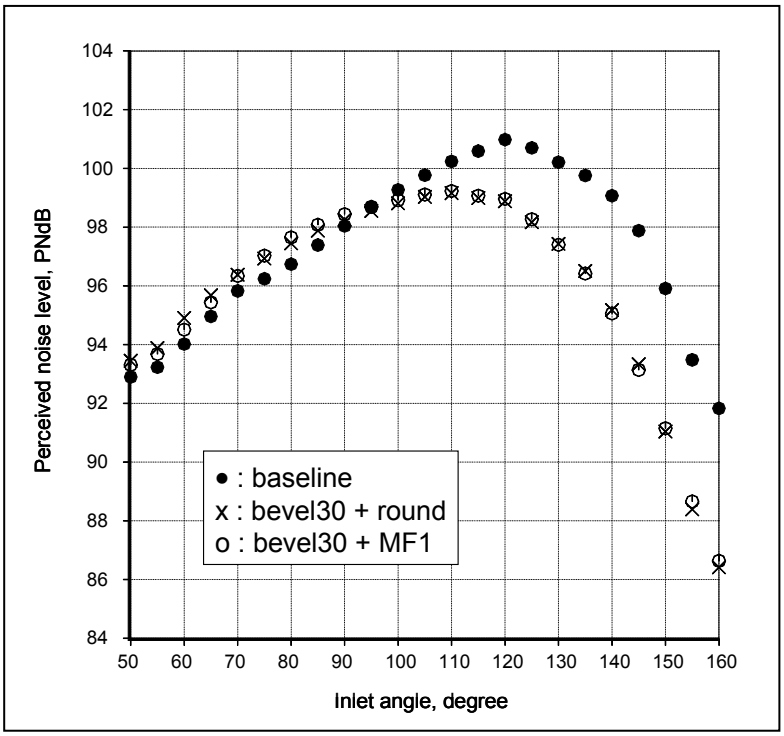

Figure 33. Variation of Perceived Noise Level with angle. NPR_p=1.71, T_p/T_a=3.16, NPR_s=1.76, T_s/T_a=1.24. •: baseline; x: bevel30+round; o: bevel30+MF1. $\phi = 0°$. M_t=0.20.

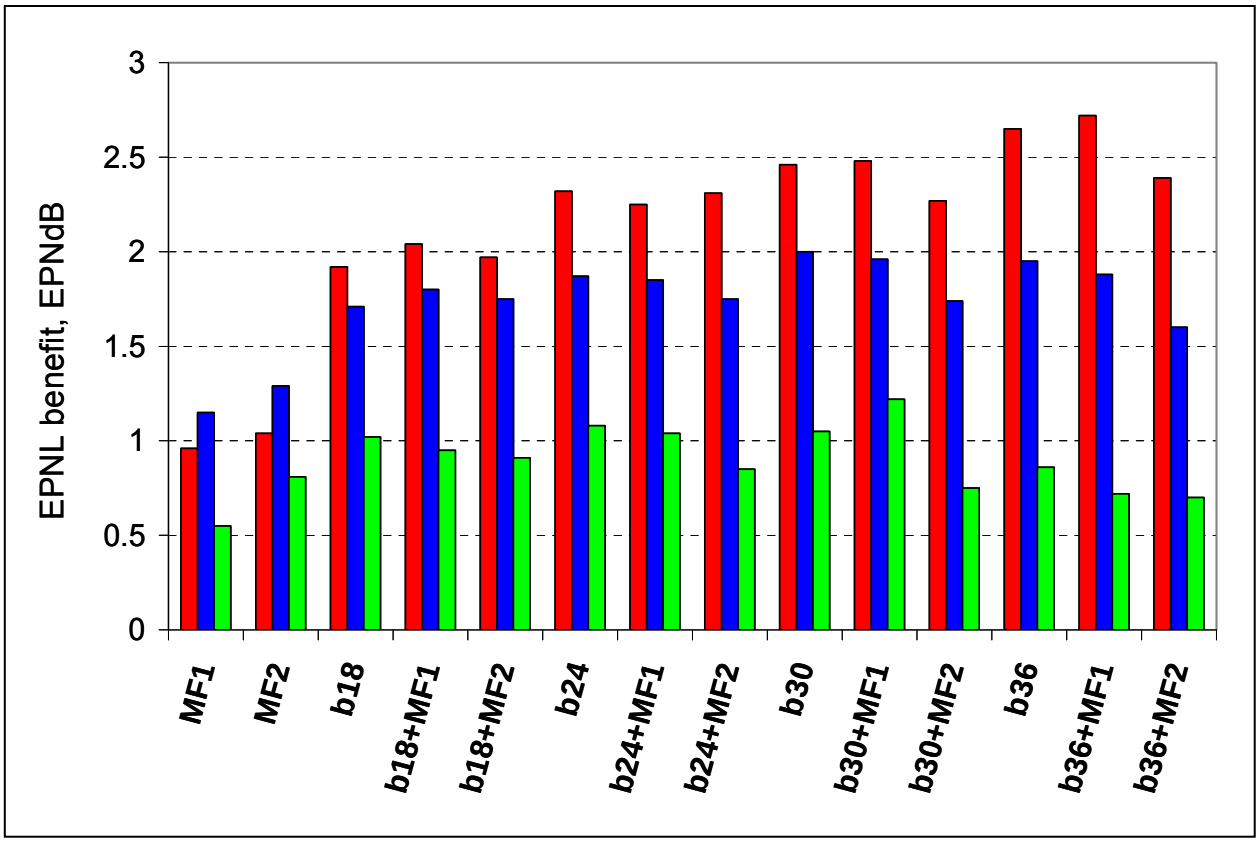

Figure 34. EPNL benefit for various nozzle geometries. NPR_p=1.71, T_p/T_a=3.16, NPR_s=1.76, T_s/T_a=1.24. $\phi = 0°$. Red: M_t=0.0; blue: M_t=0.20; green: M_t=0.28.